Extracellular transglutaminase-2, nude or associated with astrocytic extracellular vesicles, modulates neuronal calcium homeostasis

Elisa Tonoli, Ivan Verduci, Martina Gabrielli, Ilaria Prada, Greta Forcaia, Clare Coveney, Maria Pia Savoca, David J. Boocock, Giulio Sancini, Michele Mazzanti, Claudia Verderio, Elisabetta A.M. Verderio

PII: S0301-0082(22)00099-5

DOI: https://doi.org/10.1016/j.pneurobio.2022.102313

Reference: PRONEU102313

To appear in: *Progress in Neurobiology*

Received date: 21 October 2021
Revised date: 15 June 2022
Accepted date: 22 June 2022

Please cite this article as: Elisa Tonoli, Ivan Verduci, Martina Gabrielli, Ilaria Prada, Greta Forcaia, Clare Coveney, Maria Pia Savoca, David J. Boocock, Giulio Sancini, Michele Mazzanti, Claudia Verderio and Elisabetta A.M. Verderio, Extracellular transglutaminase-2, nude or associated with astrocytic extracellular vesicles, modulates neuronal calcium homeostasis, *Progress in Neurobiology,* (2021) doi:https://doi.org/10.1016/j.pneurobio.2022.102313

Extracellular transglutaminase-2, nude or associated with astrocytic extracellular vesicles, modulates neuronal calcium homeostasis

Elisa Tonoli[1], Ivan Verduci[2], Martina Gabrielli[3], Ilaria Prada[3], Greta Forcaia[4], Clare Coveney[5], Maria Pia Savoca[1], David J. Boocock[5], Giulio Sancini[4,6], Michele Mazzanti[2], Claudia Verderio[3,6*], Elisabetta A.M. Verderio[1,7*]

[1]School of Science and Technology, Centre for Health, Ageing and Understanding of Disease, Nottingham Trent University, Nottingham NG11 8NS, United Kingdom.

[2]Department of Bioscience, University of Milan, Milano 20133, Italy.

[3]CNR Institute of Neuroscience, Vedano al Lambro 20854, Italy.

[4]Human Physiology Lab., School of Medicine and Surgery, University of Milano-Bicocca, Monza 20900, Italy.

[5]School of Science and Technology, The John van Geest Cancer Research Centre, Nottingham Trent University, Nottingham NG11 8NS, United Kingdom.

[6]NeuroMI (Milan Center for Neuroscience), School of Medicine and Surgery, University of Milano-Bicocca, Monza 20900, Italy.

[7]Biological Sciences Department (BiGeA), University of Bologna, Bologna 40126, Italy

*Elisabetta A.M. Verderio

School of Science and Technology, Nottingham Trent University

Clifton lane, Nottingham, NG11 8NS, United Kingdom

tel.: +44 (0)115 848 6628; fax: +44 (0)115 848 6636

Email: elisabetta.verderio-edwards@ntu.ac.uk

*Claudia Verderio

CNR Institute of Neuroscience,

via Follereau 3,

20854 Vedano al Lambro (MB), Italy

tel.: +33 02 64488386

Email: c.verderio@in.cnr.it

Abstract

We have uncovered a novel role for astrocytes-derived extracellular vesicles (EVs) in controlling intraneuronal Ca^{2+} concentration ($[Ca^{2+}]_i$) and identified transglutaminase-2 (TG2) as a surface-cargo of astrocytes-derived EVs. Incubation of hippocampal neurons with primed astrocyte-derived EVs have led to an increase in $[Ca^{2+}]_i$, unlike EVs from TG2-knockout astrocytes. Exposure of neurons or brain slices to extracellular TG2 promoted a $[Ca^{2+}]_i$ rise, which was reversible upon TG2 removal and was dependent on Ca^{2+} influx through the plasma membrane. Patch-clamp and calcium imaging recordings revealed TG2-dependent neuronal membrane depolarization and activation of inward currents, due to the Na^+/Ca^{2+}-exchanger (NCX) operating in the reverse mode and indirect activation of L-type VOCCs, as indicated by VOCCs/NCX pharmacological inhibitors. A subunit of Na^+/K^+-ATPase was selected by comparative proteomics and identified as being functionally inhibited by extracellular TG2, implicating Na^+/K^+-ATPase inhibition in NCX reverse mode-switching leading to Ca^{2+} influx and higher basal $[Ca^{2+}]_i$. These data suggest that reactive astrocytes control intraneuronal $[Ca^{2+}]_i$ through release of EVs with TG2 as responsible cargo, which could have a significant impact on synaptic activity in brain inflammation.

Keywords: astrocytes; calcium homeostasis; extracellular vesicles; hippocampal neurons; transglutaminase-2

1. Introduction

The regulation of Ca^{2+} is a fundamental biological process in neurons, with Ca^{2+} signaling as the basis of synaptic plasticity, neurons survival and their ability to communicate (Catterall & Few, 2008; Marambaud et al., 2009). In neurons basal Ca^{2+} levels are tightly regulated within a narrow physiological range (Carafoli, 1987; Jones & Keep, 1988), and a rise in intracellular Ca^{2+} concentration ($[Ca^{2+}]_i$) is the major trigger of neurotransmitter release from nerve endings. Propagation of action potentials and membrane depolarization (~20 mV) produces Ca^{2+} influx through voltage-dependent Ca^{2+} channels which reaches micromolar levels at highly localized presynaptic sites in axons (Forti et al., 2000). Since the smallest change in Ca^{2+} currents can have a dramatic impact on neuronal function, Ca^{2+} influx is controlled by the action of Ca^{2+} membrane transporters at the plasma membrane, such as the Ca^{2+} pump ATPase and the sodium/calcium (Na^+/Ca^{2+})-exchanger (NCX), and it is buffered by a large set of

Ca^{2+} binding proteins which act as modulators of cellular Ca^{2+} transients. Extensive literature indicates that Ca^{2+} dyshomeostasis in neurons is linked with aging and neurodegeneration. In familial Alzheimer's disease (AD), autosomal dominant presenilin 1 and presenilin 2 mutations have been linked with reduction of store-operated Ca^{2+} entry and/or content of intracellular stores, causing dysregulation of Ca^{2+} homeostasis (Greotti et al., 2019). However, mechanism(s) leading to $[Ca^{2+}]_i$ alterations are still not completely clear (Nikoletopoulou & Tavernarakis, 2012; Oh et al., 2013).

Transglutaminase-2 (TG2) is a Ca^{2+}-dependent crosslinking enzyme known to be involved in multiple neurodegenerative diseases linked to Ca^{2+} dysregulation (Grosso & Mouradian, 2012), as well as a variety of conditions triggered by inflammatory processes, such as wound-healing and tissue fibrosis (Verderio et al., 2015). The implication of TG2 was first suggested by the observation that the enzyme, in the presence of activating $[Ca^{2+}]_i$, is able to crosslink pathogenic misfolded proteins typical of neurodegenerative conditions (e.g. amyloid-β and α-synuclein), thus favoring formation of protein aggregates (Andringa et al., 2004; Benilova et al., 2012; Grosso et al., 2014; Hartley et al., 2008; Junn et al., 2003). However a number of recent observations, such as the potentiation of Ca^{2+}-induced hippocampal damage by TG2 in mice brain and higher sensitivity to kainic acid-induced seizures (Tucholski et al., 2006), as well as the neurotoxic role of astrocytic TG2 following acute brain injury (Feola et al., 2017; Monteagudo et al., 2018), have hinted to a possible role of TG2 in excitotoxicity-induced neuronal cell death, which may be either consequent to $[Ca^{2+}]_i$ increases or, as a new hypothesis, triggered by TG2-mediated changes in $[Ca^{2+}]_i$. Astrocytes are an abundant source of TG2, which is externalized and accumulates in the extracellular matrix (ECM) in response to inflammatory stimuli (Pinzon et al., 2017). Importantly, astrocytes are key mediators of brain immune responses (Colombo & Farina, 2016) and TG2 has been shown to play a role in neuroinflammation (Ientile et al., 2015). Astrocytes control synapses either by direct contact and/or by secreted factors, released as single molecules or packaged into extracellular vesicles (EVs), which target pre- and post-synapses thus regulating synaptic behavior (Farhy-Tselnicker & Allen, 2018). In this study we have hypothesized that extracellular TG2 could disrupt Ca^{2+} homeostasis in neurons. We have uncovered a new role for extra-neuronal TG2, released by reactive astrocytes via EVs, in increasing neuronal $[Ca^{2+}]_i$, and shown that this occurs through NCX operation in the reverse mode and the opening of L-type VOCCs via regulation of Na^+/K^+-ATPase activity. This process is a novel example of neuron-regulation by astrocytes-derived EVs cargo under both physiological and neuroinflammatory conditions.

2. Materials and Methods

2.1. ***Primary cultures***: primary cultures of hippocampal neurons were established from E18 Sprague Dawley rat embryos or E18 C57BL6 mouse embryos as previously described (Gabrielli et al., 2015). After 14-21 days in vitro (DIV), the cultures contain a significant percentage of astrocytes (Verderio et al., 1999). Primary astrocytes from C57BL/6 WT and TG2 knockout ($TG2^{-/-}$ or TG2KO) P3 mouse pups were established as previously described (Gabrielli et al., 2015). TG2KO mice were originally obtained from Gerry Melino (De Laurenzi & Melino, 2001) and fully backcrossed as previously described (Scarpellini et al., 2014). For TG2 cell-surface activity assay, primary astrocytes were obtained from BrainBits (BrainBits, Springfield, IL, USA) and processed following the manufacturer's protocol.

2.2. ***Reagents***: guinea pig liver TG2 (Zedira GmbH, Darmstadt, Germany) 30 µg/ml apart from when indicated in the figure legend; LPS (Sigma-Aldrich, St. Louis, MO, USA) 1 µg/ml; TTX (Tocris, Bristol, United Kingdom) 1 µM; BOCDON (Zedira) 200 µM; Nifedipine (Sigma-Aldrich) 1 µM; Cadmium (Sigma-Aldrich) 200 µM; Nickel (Sigma-Aldrich) 100 µM; YM-244769 (Tocris) 1 µM; APV (Tocris) 50 µM; CNQX (Tocris) 10 µM; biotin-cadaverine (Sigma-Aldrich) 0.1 mM; apyrase (Sigma-Aldrich) 30 U/ml; human fibronectin (Sigma-Aldrich) 5 µg/ml; ATPase from porcine cerebral cortex (Sigma-Aldrich) 0.5 mU; Ouabain (Tocris) 1 mM.

2.3. ***Immunocytochemical staining***: Cells were fixed in 4% paraformaldehyde - 4 % sucrose (w/v) and immunofluorescence staining was performed using the following antibodies: mouse monoclonal anti-TG2 (IA12 – Tim Johnson, University of Sheffield (Scarpellini et al., 2014)), guinea pig anti-VGLUT1 (Synaptic System, Goettingen, Germany), rabbit anti-GFAP (Dako, Agilent, Santa Clara, CA, USA), rabbit anti-Shank2 (Synaptic System), rabbit anti-Fibronectin (Sigma-Aldrich), rabbit anti-β-tubulin (Sigma-Aldrich) and rabbit anti-NR2B (Alomone, Jerusalem, Israel). Secondary antibodies were conjugated with Alexa-488, Alexa-555 and Alexa-633 fluorophores (Invitrogen). Further details are available in the Supplementary Table A1. Coverslips were visualized by laser scanning Leica SP5 confocal microscope using 63X oil immersion objective. Successive serial optical sections (0.5 µm) were recorded over 5 µm planes and maximum projections were selected for quantification. Fluorescence intensity and co-localization were estimated using the Leica LAS AF Lite software or ImageJ software as indicated in the Supplementary Extended methods.

2.4. ***Synaptosomes preparation:*** Two adult mouse cortices were homogenised in 20 ml/g of tissue of TS buffer (320 mM sucrose in Tris/HCl 10 mM, pH 7.4), using a glass-Teflon homogeniser on ice. Brain homogenates were then centrifuged at 1,000xg for 5 min at 4^{o}C. The supernatant was layered over a discontinuous Percoll density gradient prepared according to Dunkley et al. (Dunkley et al., 2008), one gradient per cortex. The gradient was centrifuged at 33,000xg for 5 min at 4^{o}C using a MLA-50 fixed-angle rotor (Beckman). The synaptosomal fraction was collected, diluted in KRH and centrifuged at 20,000xg for 10 min, the pellet resuspended in RIPA buffer and stored at -80^{o}C pending use.

2.5. ***Western blotting***: Samples were electrophoresed on 10% SDS polyacrylamide gels according to standard procedures. The following antibodies were used: mouse monoclonal anti-TG2 (IA12), anti-FLOT-2 (BD Biosciences, Wokingham, United Kingdom), anti-PSD-95 (Neuromab, Davis, C, USA), anti-TOM20 (Santa Cruz, Dallas, Texas, USA) and polyclonal rabbit anti-TG2 (ab421) (Abcam), anti-β-tubulin (Abcam), anti-α-tubulin (Sigma-Aldrich), anti-ALIX (Covalab, Bron, France), anti-NR2B (Alomone, Jerusalem, Israel), anti-VGAT (Synaptic systems, Goettingen, Germany), anti-VGLUT1 (Synaptic systems), anti-GFAP (GeneTex). Further details are available in Supplementary Table A1. Blots were developed using enhanced chemiluminescence (SuperSignal West Femto Maximum Sensitivity Substrate, Thermo Fisher Scientific) and protein band intensity was quantified by Aida Image Analyzer v.4.03 (Raytest, Germany).

2.6. ***Isolation of extracellular vesicles (EVs)***: EVs were isolated from conditioned medium (CM) of astrocytes by differential centrifugation at 110,000xg as previously described (Furini et al., 2018; Prada et al., 2018). The 10,000xg centrifugation was omitted to pellet large and small EVs together. Each astrocytes preparation derived from ≥10 mouse P3 pups. Specifically, 80% confluent monolayers were washed twice with PBS or KRH and incubated in serum-free media in the presence or absence of lipopolysaccharide (LPS, 1 µg/ml), for 24 h. CM was collected and supplemented with protease inhibitors before centrifugation. EVs were resuspended either intact in particle-free PBS (for Nanoparticle Tracking Analysis, TEM and TG2 activity assay) or KRH (for Ca^{2+} imaging) or lysed in RIPA buffer (for western blotting) or lysis buffer (0.25 M sucrose, 2 mM EDTA, 5 mM Tris-HCl, pH 7.4) (for TG2 activity assay). Of note, the immunogenicity of glia-derived EVs is very low and the effects of EVs from mouse cultures can be tested on either rat or mouse neurons (Antonucci et al., 2012).

2.7. ***Nanoparticle tracking analysis:*** Nanoparticle tracking analysis (NTA) was performed using ZetaView PMX 120 (Particle Metrix, Meerbusch, Germany) and its corresponding software (ZetaView 8.04.02) to examine EVs size distribution and concentration. EVs samples, resuspended in particle-free PBS, were diluted to reach 50-200 particles/frame and analyzed with a flow cell sensitivity of 80% across two cycles of 11 positions/cycle.

2.8. ***ExoView analysis***: The ExoView R200 platform (NanoView Biosciences, Malvern, United Kingdom) was used to characterize surface markers of EVs from WT and TG2KO astrocytes. Conditioned medium (serum-free) was collected after 24h from ~70% confluent T175 flasks, centrifuged at 2,500xg 4^{o}C for 10 min and then concentrated ~80 times using Amicon Ultra 50K MWCO centrifugal filters (Sigma-Aldrich). Concentrated medium was diluted 1:2 in incubation buffer for analysis with the ExoView R200 platform (human tetraspanin kit) following the manufacturer instructions for detection of CD9 positive EVs. Following capturing of EVs on mouse tetraspanin chips, validated by measurement of CD9 and CD81 or control IgGs, EVs-associated TG2 was immunolabelled by Alexa Fluor 555-conjugated anti-mouse TG2 antibody IA12 (Antibody labelling kit, Life Technologies, Carlsbad, CA, USA) following the manufacturer instructions.

2.9. ***Density gradient***: EVs were isolated as described before, resuspended in 25 mM Trehalose in PBS, loaded on top of a density gradient (5%, 20% and 40% w/v) Optiprep iodixanol solution in 25 mM Trehalose/PBS (Sigma-Aldrich) and centrifuged at 236,000xg at 4^{o}C for 5h using a swinging-bucket rotor (SW 40 Ti, Beckman). Ten fractions were collected from top to bottom, diluted in PBS and ultracentrifuged at 110,000xg at 4^{o}C for 70 min (Chen et al., 2020). Pellets were resuspended in RIPA buffer for western blotting analysis.

2.10. ***Transmission Electron Microscopy:*** EVs isolated from untreated WT astrocytes were analyzed by Transmission Electron Microscopy (TEM) as previously described (Charrin et al., 2020), with a few modifications. Briefly, EVs were deposited for 20 min on formvar/coated 200 mesh nickel EM grids (TAAB Laboratories Equipment Ltd, Berks, United Kingdom). Then grids were fixed with 2% paraformaldehyde/phosphate buffer pH 7.4 and processed for negative staining or single immunogold labelling. EVs were stained with rabbit monoclonal anti-CD63 (Abcam) or anti-TG2 antibody (IA12 and Ab80653) followed by 6 nm colloidal gold anti-mouse IgG or 18 nm colloidal gold anti-rabbit IgG (Jackson Immunoresearch Europe, Ely, United Kingdom). The negative staining was performed using a mixture of uranyl acetate/methylcellulose as previously described (Slot & Geuze, 2007). Brightfield transmission

electron micrographs of the stained EVs were taken at an indicated magnification of 40,000x using a JEM-2100Plus (JEOL, Herts, United Kingdom) TEM operating at an accelerating voltage of 80 kV, digital micrographs recorded using a Rio 16 CMOS camera using GMS 3.0 (Gatan, Pleasanton, CA, USA).

2.11. ***Total TG activity assay:*** transglutaminase activity of EVs either intact (resuspended in PBS) or lysed (resuspended in mild lysis buffer: 0.25 M sucrose, 2 mM EDTA, 5 mM Tris-HCl, pH 7.4) was measured through incorporation of biotin cadaverine (BTC, Sigma-Aldrich) into FN as previously described (Furini et al., 2018). Samples were incubated in either lysis buffer or PBS pH 7.4 for 15h at +4ºC and then assayed in duplicates (N=3 independent experiments). TG2 activity was calculated by removing the absorbance values obtained from the respective buffer (either PBS or lysis buffer) and expressed as mU/µg of protein.

2.12. ***Cytoplasmic calcium imaging***: Intracellular Ca^{2+} levels were assessed in hippocampal neurons loaded with Fura-2/AM dye (Merck, Darmstadt, Germany) as previously described (Joshi et al., 2014) and explained in the Supplementary Extended methods. Neurons were distinguished from astrocytes by morphology and response to KCl stimuli (Bacci et al., 1999). Experiments were performed in Krebs–Ringer's HEPES solution (KRH) (125 mM NaCl, 5 mM KCl, 1.2 mM $MgSO_4$, 1.2 mM KH_2PO_4, 2 mM $CaCl_2$, 6 mM d-glucose, and 25 mM HEPES/NaOH, pH 7.4), whereas in some cases Na^+/K^+-free KRH was used instead, where both NaCl and KCl were isosmotically substituted for choline chloride. Ca^{2+} concentration was expressed as F340/380 fluorescence ratio as explained in the Supplementary Extended methods. For each experiment, N indicates the total number of analyzed neurons, either from multiple slides of the same cell preparation or from different preparations. Each neuronal preparation derived from ≥10 rat E18 embryos.

2.13. ***Calcium imaging in brain slices:*** Slices were obtained from 10 days old CD1 mice and prepared as explained in the Supplementary Extended methods. Acquisition protocols consisted of 1.2 fps time-lapse sequences of Fura-2 fluorescence with 30 ms exposure time. ROI over the field of view were selected, and the mean pixel intensity at each frame was measured. After 3 min baseline recording, 30 µg/ml TG2 (Zedira) in ACSF was perfused until plateau of the response was reached, then washed out. Analysis was performed using Metafluor software (Molecular Devices, San Jose, CA, USA).

2.14. ***Transient transfection***: 8 DIV (days in vitro) neurons were transfected with 1.5 µg of pEGFP-N1 vector (Clontech Laboratories, Takara Bio Inc., Mountain View, CA, USA) or pEGFP-N1-TG2 vector (Furini et al., 2018) using 6 µl of Lipofectamine2000 (Thermo Fisher Scientific) in a total volume of 100 µl per slide (about

$1.7x10^5$ neurons). After 45 min incubation, transfected neurons were washed with Neurobasal medium and incubated in filtered conditioned neuronal medium for 48 h before analysis.

2.15. ***Whole cell patch clamp*****:** Patch clamp experiments were performed in current clamp and voltage clamp configurations as explained in the Supplementary Extended methods. For current clamp experiments, the effect of TG2 (30 µg/ml) on neuron resting potential was examined. Voltage clamp experiments were performed to observe the involvement of Voltage Operated Calcium Channels (VOCCs) in the phenomenon. Specifically, L-type VOCCs were isolated with a pre-pulse of 40 mV and a Δ10 mV step protocol from -30 to 0 mV.

2.16. ***Isolation of TG2 complexes and Data Acquisition by Mass Spectrometry.*** TG2-associated proteins were isolated from hippocampal neurons incubated with 30 µg/ml TG2 in KRH buffer for 5 min and from untreated neurons as control (N=3). After incubation, the supernatant was removed and neurons were lysed using IP buffer (25 mM Tris-HCl, 150 mM NaCl, 1 mM EDTA, 1% [v/v] NP40 detergent solution, and 5% [v/v] glycerol, pH 7.4) containing protease inhibitor cocktail (Sigma-Aldrich). The whole cell lysate was centrifuged at 13,000xg for 10 min at 4°C to remove larger particulates. TG2 with associated proteins was immunoprecipitated from cell lysates and supernatants as previously described (Furini et al., 2018) with few modifications. Incubation of samples with the anti-TG2 antibody-coated beads (CUB7402; Thermo Fisher Scientific) was performed for 20 h at 4°C in constant rotation. Proteins were reduced, alkylated and trypsin digested directly on the beads and peptides were analyzed by RP-HPLC-ESI-MS/MS using a TripleTOF 6600 mass spectrometer (SCIEX) in data-dependent acquisition mode for spectral library construction, and in SWATH 2.0 data-independent acquisition mode using 100 variable SWATH acquisition windows for quantification as described in the Supplementary Extended methods. The mass spectrometry proteomics data have been deposited to the ProteomeXchange Consortium via the PRIDE (Perez-Riverol et al., 2019) partner repository with the dataset identifier “PXD022224". Analysis of differentially expressed proteins was performed using the OneOmics cloud processing online platform (SCIEX) as described in the Supplementary Extended methods.

2.17. ***ATPase activity assay:*** Na^+/K^+-ATPase activity was analyzed using the High Throughput Colorimetric ATPase Assay kit (Innova Biosciences, Cambridge, United Kingdom) according to the manufacturer’s instructions. Briefly, ATPase isolated from porcine cerebral cortex (0.5 mU/well) was assayed in the

presence or absence of gplTG2 (0.5 mU/well) and specific Na^+/K^+-ATPase inhibitor ouabain (1 mM) in reaction buffer (50 mM Tris-HCl, 100 mM NaCl, 25 mM KCl, 3 mM $MgCl_2$, 2 mM $CaCl_2$, 0.5 mM ATP) (modified from (Gable et al., 2017)). Samples were incubated for 30 minutes at room temperature, then the reaction was stopped by addition of the P_iColorLock mix, followed by a stabilizer. The plate was read at 595 nm after 30 minutes.

2.18. ***Statistical analysis***: All data are presented as mean ± SD from the indicated number of independent experiments (N=3) or cells as indicated in the respective figure legends. Each primary cell preparation was derived from ≥10 rat E18 embryos (hippocampal neurons) or ≥10 mouse P3 pups (astrocytes). Data in each experiment were first tested for normal distribution by D'Agostino-Pearson normality test (GraphPad Prism 7.05 software). In the case of normally distributed data, statistical analysis was performed by Student's t-test (2 groups comparisons) or one-way Anova (Tukey multiple comparisons test). In the case of non-normally distributed data, statistical analysis was performed by nonparametric Mann-Whitney test (2 groups comparisons) or Kruskal-Wallis Dunn's test (multiple comparisons). For paired normalized data, the Wilcoxon matched-pairs signed rank test was used. Differences are considered significant by $p<0.05$.

3. Results

3.1. TG2 released by primary astrocytes in association with EVs increases $[Ca^{2+}]_i$ in neurons

Previous studies have shown that astrocytes are a main source of extracellular TG2 in the brain, particularly in situations of inflammation/astroglial response to injury (Colak & Johnson, 2012; Monteagudo et al., 2018; Pinzon et al., 2017; Quinn et al., 2018). A granular pattern of TG2 distribution was detected by immunofluorescence in either permeabilized or non-permeabilized fixed cultures of astrocytes, suggesting that TG2 has a predominant extracellular location in astrocytes (Fig. 1A). Evaluation of endogenous cell surface TG2 by an optimized activity assay revealed high extracellular TG2 activity (sensitive to the specific inhibitor ZDON) in cultured astrocytes (Supplementary Fig. A1). Conversely in hippocampal neurons, TG2 showed a significantly higher staining in permeabilized cells (Fig.1B), where it partially localized at synaptic sites, as indicated by co-staining with the pre- and post-synaptic markers VGLUT1 (blue) and SHANK2 (red) (Fig. 1C). Western blotting analysis of synaptosomes from adult mouse brain (Fig. 1D) suggested the presence of TG2 at synaptic sites *in vivo*.

Once externalized at the astrocyte surface TG2 can bind to matrix fibronectin (FN) (Pinzon et al., 2017) and our data confirmed a partial co-localization of TG2 with FN (Supplementary Fig. A2). We hypothesized that TG2 may

be released via extracellular vesicles (EVs), as recently described in other cell systems (Antonyak et al., 2011; Diaz-Hidalgo et al., 2016; Furini et al., 2018). In this form, TG2 could travel to neurons, unless released from astrocytes in direct contact with synapses. To test this possibility, astrocyte-derived EVs were isolated from conditioned medium of primary astrocytes obtained from wild type ($TGM2^{+/+}$) and knockout ($TGM2^{-/-}$) mouse brain (De Laurenzi & Melino, 2001). Characterization by Nanoparticle tracking analysis (Fig. 2A), TEM (Fig. 2B), Tetraspanin phenotyping (CD9) (Fig 2C), detection of vesicular marker ALIX and Flotillin-2, two luminal proteins, and prion protein (PrP), a GPI-anchor protein highly enriched in astrocyte-derived EVs, absence of two cytosolic proteins (GFAP and Tubulin) and absence of mitochondrial marker TOM20 confirmed the size, morphology and vesicular cargo of EVs (Fig. 2D). NTA showed a trend increase in EVs number upon LPS treatment (Fig. 2A). Neither average particle number nor mode size were significantly different between WT and TG2KO cells, either untreated or LPS-treated (Fig. 2A-I and 2A-II), whereas a significant difference was observed between WT and WT+LPS particle number when looking at specific sizes (45-195 nm range) (Fig. 2A-III). TEM analysis and immunogold labelling of WT vesicles showed that they had the expected cup shape and confirmed the presence on the EVs surface of specific EVs marker CD63 and of TG2 (Fig. 2B). Western blotting analysis of astrocytes-derived EVs lysates revealed the presence of TG2 protein in WT EVs (Fig 2D-I) which displayed a trend increase upon pro-inflammatory stimulation with LPS (TG2 immunoreactivity normalized over control: 1.35±0.19, Fig. 2D-II). Furthermore, negligible TG2 was detected in EVs-depleted supernatants after recovering all proteins by TCA precipitation (Fig. 2D), especially after using a higher ultracentrifugation speed, that ensured efficient depletion of flotillin positive EVs (Fig. 2D-I). These data show for the first time that TG2 is released from cultured astrocytes as a cargo of EVs under both resting physiological and stimulated (inflammatory) conditions. An ALIX immunoreactive band of slightly lower molecular mass was present in EVs-depleted supernatants, which likely represents a cleavage form of soluble ALIX, as previously suggested (Pan et al., 2008). The association of TG2 with EVs was confirmed by density gradient centrifugation (Fig. 2D-III). EVs markers FLOT-2 and ALIX were predominant in fraction 4, and TG2 was present in the same EVs-rich fraction. The localization of TG2 in EVs was investigated using a sensitive enzymatic assay as we previously described (Furini et al., 2018). TG2 was detected at comparable levels in both intact EVs and EVs lysed in sucrose-lysis buffer (Fig. 2E-I). The background TG activity in the TG2KO EVs is likely due to compensatory events by other TG family members (De Laurenzi & Melino, 2001). Moreover, pre-incubation of intact EVs with non membrane-permeable TG2 inhibitor BOCDON, led

to a significant decrease in TG2 activity, suggesting a predominant surface location of TG2 (Fig. 2E-II). To corroborate this further, astrocytic EVs were captured by tetraspanin antibodies immobilised on a microarray chip, directly from concentrated serum-free conditioned medium (Supplementary Fig. A3). TG2 was detected on the CD9 and CD81-immobilised EVs populations by fluorescently tagged mouse anti-TG2 antibody (IA12). There was negligible EVs binding and TG2 detection on control IgGs, further suggesting that TG2 is displayed on the EVs surface.

To investigate the involvement of the astrocytes EVs TG2 cargo on neuronal function, the modulation of $[Ca^{2+}]_i$ by EVs isolated from WT and TG2KO LPS-primed astrocytes was monitored in fura-2-loaded hippocampal neurons. In order to exclude variations in $[Ca^{2+}]_i$ due to vesicular ATP leaking from astrocyte-derived EVs (D'Arrigo et al., 2021), the assay was performed in the presence of the ATP degrading enzyme apyrase. As shown in Fig. 2F-I, TG2-containing EVs (EVs WT) were able to rise basal $[Ca^{2+}]_i$, whereas addition of TG2KO EVs did not cause significant changes. Further, pre-incubation of WT EVs with monoclonal anti-TG2 antibody IA12 led to a significantly lower calcium increase in hippocampal neurons (Fig 2F-II). This treatment significantly decreased adhesion of EVs to the neuron surface (Supplementary Fig. A4; Supplementary Movie 1 and 2), thereby inhibiting the ability of vesicular TG2 to rise neuronal $[Ca^{2+}]_i$. In this experiment, EV-neuron interaction was monitored by delivering single EVs to neurons by optical manipulation and imaging their interaction dynamics in bright field (D'Arrigo et al., 2021). These data have two novel implications: that astrocytes-derived EVs concur to the regulation of neuronal Ca^{2+} homeostasis and that TG2, which is exposed on the surface of astrocytes-derived EVs, is responsible for this specific function.

3.2. Extracellular TG2 increases cytoplasmic calcium concentration, both in cultured neurons and hippocampal slices

To gain insights into the mechanism leading to increased neuronal $[Ca^{2+}]_i$ by extracellular TG2 we next monitored neuronal $[Ca^{2+}]_i$ dynamics upon addition to the extracellular solution of purified TG2 (from guinea pig liver, 10-30 µg/ml). Differentiated hippocampal neurons often exhibit synchronous Ca^{2+} oscillations in the soma, reflecting burst of neuronal firing (Bacci et al., 1999). Incubation with purified TG2 promoted the onset of a synchronous Ca^{2+} spike and increased the interspike $[Ca^{2+}]_i$, leading to blockage of oscillatory activity (Fig. 3A-I, “TG2”). Upon TG2 removal by wash with KRH (Fig. 3A-I, “Wash”), interspike $[Ca^{2+}]_i$ decreased to pre-treatment values and

spontaneous Ca^{2+} oscillations re-started, indicating that the action of soluble TG2 was reversible. To further examine the action of TG2 on $[Ca^{2+}]_i$, neurons were exposed to TG2 in the presence of TTX (1 µM), which prevents spontaneous synaptic and synchronous Ca^{2+} activity. In virtually all rat neurons tested, addition of TG2 led to a small but highly significant increase in $[Ca^{2+}]_i$ in the neuron cell bodies (Fig. 3A-II, "TG2"), while no $[Ca^{2+}]_i$ changes were observed in astrocytes present in the cultures. Similar raises in $[Ca^{2+}]_i$ were observed in mouse hippocampal neurons upon TG2 exposure in the presence of TTX (Fig. 3B). Moreover, pre-incubation of TG2 with monoclonal antibody Cub7402 or IA12 led to a significant decrease in $[Ca^{2+}]_i$ rise compared to TG2 alone (Fig. 3B). Pre-incubation with mouse IgG control did not affect TG2-driven Ca^{2+} influxes (AUC TG2: 5.6 ± 2.3; AUC TG2+IgG: 8.8 ± 4, p=NS). This confirmed that the changes in basal $[Ca^{2+}]_i$ elicited by exogenous TG2 were specific. To rule out that the phenomenon was only found in dissociated cultures, we investigated the effect of TG2 on hippocampal slices. Similar Ca^{2+} response was evoked by TG2 in neurons in mouse hippocampal slices loaded with fura-2 when the TG2 protein was added in perfusion mode (Fig. 3C). In order to clarify whether extracellular TG2 increases basal Ca^{2+} levels by enhancing Ca^{2+} influx into neurons, we exposed cultured neurons to purified TG2 in Ca^{2+}-free solution (Fig. 3D-I). No rise in basal $[Ca^{2+}]_i$ occurred in Ca^{2+}-free conditions, while TG2-dependent Ca^{2+} rises were clearly recorded from the same neurons after addition of Ca^{2+} ions (2mM Ca^{2+}) to the extracellular medium (Fig. 3D-II). This establishes that the $[Ca^{2+}]_i$ rise evoked by exogenous TG2 is mediated by Ca^{2+} influx from the extracellular environment through the plasma membrane. Interestingly, the action of TG2 was reversible, as observed in the absence of TTX (Fig. 3A-I) and neurons recovered basal $[Ca^{2+}]_i$ upon removal of the protein ("Wash") from the extracellular solution (Fig. 3A-I, 3A-II and 3B). This finding implies that the observed process might not be due to transamidation, which leads to a covalent irreversible modification of protein substrates and should not disappear once TG2 is removed. To analyze this further, we tested the activity of exogenous TG2 added to hippocampal neurons during calcium imaging recordings and found that it was catalytically inactive in the same experimental conditions of the calcium imaging, unless activated by supplementation of a reducing agent (Supplementary Fig. A5). Notably, we previously showed that extracellular TG2 bound to the ECM is catalytically inactive or poorly active in the absence of a reducing agent (Verderio et al., 2003).

We next asked whether TG2 secreted/externalized from neurons could rise basal $[Ca^{2+}]_i$ similarly to exogenous/astrocyte-derived TG2. To this aim, we first transfected hippocampal neurons with TG2 and measured

$[Ca^{2+}]_i$. Transfected cells (pEGFP-N1-TG2) displayed an increase in resting $[Ca^{2+}]_i$ compared to control neurons (pEGFP-N1) (Fig. 4A). This could suggest that upon over-expression, neuronal TG2 may act extracellularly in an autocrine manner, controlling basal $[Ca^{2+}]_i$, albeit we cannot exclude an intracellular action of the protein. Treatment of the transfected cells with BOCDON, a non-permeable inhibitor of TG2, did not affect changes in $[Ca^{2+}]_i$ evoked by the transfected TG2 (Fig. 4B), thus inhibition of extracellular TG2 does not affect intracellular Ca^{2+} changes in transfected neurons. As testing the transamidating activity of TG2 solubilized in the extracellular saline confirmed that it is predominantly inactive, unless treated with a reducing agent (Supplementary Fig. A5), and we know that intracellularly TG2 transamidation is largely silent (Verderio et al., 1998), we conclude that TG2 evoking Ca^{2+} responses is prevalently inactive as a protein crosslinker. However, we cannot exclude that also the TG2 overexpressed intracellularly might be involved.

3.3. Extracellular TG2 causes calcium influx through L-type VOCCs

We next asked how extracellular TG2 promotes Ca^{2+} influx through the plasma membrane. Neurons were stimulated with exogenous TG2 in the presence of blockers of the main Ca^{2+} entry pathways in neurons, namely glutamate receptors and VOCCs. The NMDA receptor antagonist APV and the AMPA/kainate receptor antagonist CNQX did not affect Ca^{2+} increase upon TG2 addition, ruling out the involvement of these ligand-gated Ca^{2+} permeable receptors in the process (Fig. 5A-I and 5A-II). To analyze the possible contribution of VOCCs, we used a selection of pharmacological inhibitors of these channels. Pre-treatment with cadmium, a general blocker of VOCCs, reduced TG2-dependent Ca^{2+} responses by about 82.4% (Fig. 5B-I) and caused an almost complete recovery (88.3%) of $[Ca^{2+}]_i$ towards basal levels when applied during the plateau phase of Ca^{2+} response induced by exogenous TG2 (Fig. 5C-I). Similarly, pre-treatment with nickel, a more specific inhibitor of T-type VOCCs, decreased TG2-dependent Ca^{2+} rises by 66.2% (Fig. 5B-II) while it caused a drop of $[Ca^{2+}]_i$ below basal level (151% inhibition) when applied during the plateau phase (Fig. 5C-II). The involvement of VOCCs was further indicated by the observation that Ca^{2+} transients evoked by depolarization (15 mM KCl) rose faster and reached a higher peak in the presence of extracellular TG2, with a significant increase in average Ca^{2+} influx (Fig. 5D). Among VOCCs controlling Ca^{2+} transport through the plasma membrane, L-type VOCCs are highly abundant in the somatodendritic region of hippocampal neurons (Condliffe et al., 2010; Leitch et al., 2009; Pravettoni et al., 2000). We therefore asked whether these channels might contribute to Ca^{2+} influx in the neuronal soma evoked

by exogenous TG2. We found that Ca^{2+} responses to TG2 were reduced by about 36% in neurons pre-treated with the selective of L-type blocker nifedipine (NF) (Fig. 5E-I). In addition, the drug caused a partial recovery of $[Ca^{2+}]_i$ towards resting levels when applied during the plateau phase of Ca^{2+} response induced by TG2 (Fig. 5E-II), suggesting that TG2 dependent Ca^{2+} influx partially occurs through L-type VOCCs.

3.4. Extracellular TG2 induces membrane depolarization and the generation of ionic inward currents, which are inhibited by Nifedipine

To further characterize the $[Ca^{2+}]_i$ response evoked by TG2, we performed whole cell electrophysiological recordings of hippocampal neurons. In current clamp, TG2 perfusion induced a slow membrane depolarization (of about 20 mV) (Fig. 6A-I), which was reverted by addition of nickel (Fig. 6A-II). In voltage clamp, TG2 promoted excitatory postsynaptic currents (EPSCs), consistent with the activation of an inward Ca^{2+} current (Fig. 6B). In the same configuration, analysis of the current/voltage relationship (I/V curves) using a protocol for isolation of L-type VOCCs, showed that perfusion of TG2 (Fig. 6C-I, red I/V curve) led to an increased inward current compared to control (black I/V curve), which was completely prevented by the presence of the L-type VOCCs blocker NF (Fig. 6C-II, red I/V curve compared to control black I/V curve). These data revealed L-type VOCCs as one of the possible main targets of TG2 responsible for dysregulation of basal Ca^{2+} concentration in neurons.

3.5. Contribution of the sodium/calcium exchanger to the calcium response evoked by TG2

Data so far have identified L-type VOCCs as the main channel through which extracellular TG2 induces Ca^{2+} influx and membrane depolarization. Despite electrophysiological recordings indicated complete inhibition of inward Ca^{2+} current evoked by TG2 under block of L-type VOCCs (Fig. 6C), a residual Ca^{2+} response was observed in Ca^{2+} imaging experiments, largely sensitive to both cadmium and nickel (Fig. 5E). In addition to VOCCs, both cadmium and nickel are known to inhibit the activity of the Na^+/Ca^{2+}-exchanger (NCX), a key regulator of Ca^{2+} transport through the plasma membrane. NCX normally removes Ca^{2+} from neurons in exchange for Na^+, which enters the neuron down its gradient across the plasma membrane (Blaustein & Lederer, 1999). However, perturbation of the Na^+ gradient leads to operation of NCX in the reverse mode, causing Ca^{2+} influx into the neurons (Blaustein & Lederer, 1999). To investigate the involvement of NCX in the reverse mode in TG2-induced Ca^{2+} influx, we removed Na^+ (and potassium K^+) from the extracellular saline. In these conditions,

the response to extracellular TG2 was strikingly increased (about 8-fold increase) (Fig. 7A), suggesting that NCX may amplify TG2-dependent Ca^{2+} entry. Conversely, addition of the NCX inhibitor YM-244769 significantly decreased TG2-dependent Ca^{2+} influx in both normal and Na^+-free medium (Fig. 7B), further supporting NCX contribution to Ca^{2+} elevations in neurons exposed to TG2.

3.6. Interactors of extracellular TG2 in hippocampal neurons: Na^+/K^+-ATPase inhibition by extracellular TG2.

To gain insights into the molecular interactions leading to the opening of L-type VOCCs and NCX operation by extracellular TG2 in neurons, we immunoprecipitated TG2 from the lysate and secretome of neurons treated with extracellular TG2 and analyzed the immunoprecipitated proteins by quantitative comparative proteomics relative to untreated neurons immunoprecipitates as shown in Fig. 8A (full list of proteins is available in Supplementary Table A2). Although we cannot exclude that extracellular TG2 might interact with some proteins during or after cell lysis, the TG2 interactome we generated is likely to include both direct and indirect interactors of extracellular TG2, which would explain the presence of cytosolic proteins. Among the transporters which emerged as significant TG2 partners, Na^+/K^+-transporting ATPase subunit α (AT1A3) was three times more associated with neurons exposed to extracellular TG2 (confidence 70%) (Fig. 8B). We hypothesized that AT1A3 could be part of the mechanism of Ca^{2+} influx triggered by extracellular TG2 via inhibition of Na^+/K^+-ATPase by TG2, with increase of intracellular Na^+ leading to switch of NCX in the reverse mode (Fig 7A-B). To test ATPase inhibition by TG2, ATPase activity was measured using ATPase isolated from porcine cerebral cortex either in the presence or absence of TG2 using the specific Na^+/K^+-ATPase inhibitor ouabain as a control. Incubation with TG2 led to a small but significant reduction in ATPase activity suggesting that perturbation of Na^+/K^+-transport by extracellular TG2 may trigger the rise in neuronal Ca^{2+} influx (Fig 8C).

According to our findings, reactive astrocytes control intraneuronal $[Ca^{2+}]_i$ through release of TG2 in association to extracellular vesicles (Fig. 9). Upon interaction with neurons extracellular TG2 promotes the opening of L-type calcium channels and induces the Na^+/Ca^{2+}-exchanger to operate in the reverse mode, likely through inhibition of Na^+/K^+-ATPase, setting basal $[Ca^{2+}]_i$ at higher levels and enhancing neurotransmission. These findings link astrogliosis, which typically occurs under brain inflammation and degeneration with Ca^{2+} dyshomeostasis in neurons and identifies extracellular TG2 as a key astrocyte-derived factor driving neuron dysfunction.

4. Discussion

Our study unveils a novel mechanism by which TG2 regulates Ca^{2+} homeostasis in hippocampal neurons. We show that extracellular TG2 drives Ca^{2+} influx into neurons both in culture and brain slice, via inhibition of Na^{+}/K^{+}-ATPase activity and via indirect activation of L-type VOCCS due to the depolarizing shift triggered by the Na^{+}/K^{+} blockage and NCX reversal action mode.

A key observation is that the sources of extracellular TG2 are astrocytes-derived EVs, which have TG2 as cargo displayed at the EVs surface. EVs-associated TG2 significantly increases $[Ca^{2+}]_i$ in neurons, as demonstrated by selective $[Ca^{2+}]_i$ rises in response to EVs derived from WT but not TG2KO cells. Notably, TG2 content tends to increase in EVs released by reactive astrocytes. This is consistent with published data showing higher externalization of astrocytic TG2 in response to neuroinflammation (i.e. TNF-α + IL-1β treatment) (Pinzon et al., 2017) and increased TG2 levels in association with astrogliosis, an inflammatory processes which is activated in brain in response to injury and the release of pro-inflammatory cytokines (Hostenbach et al., 2014; Ientile et al., 2015). Astrocytes play a key role in synaptic scaling, i.e. the adjustment of synaptic strength in response to prolonged changes in the electrical activity to maintain neuronal function and survival (Papouin et al., 2017). Potentiation of synaptic strength largely occurs via insertion of postsynaptic AMPA receptors driven by the release of TNFα by glial cells (Stellwagen & Malenka, 2006). However, the exact mechanism and molecular actors involved in synaptic scaling are still unknown (Papouin et al., 2017). TG2, once delivered by astrocytic EVs and thus concentrated at sites of neuronal contact, may favor excitatory transmission, thereby contributing to synaptic scale up. Further work is required to address this intriguing hypothesis.

EVs play an emerging role in neuron-glia cross-talk (Holm et al., 2018; Turola et al., 2012). In particular, astrocyte-derived EVs induce a long lasting potentiation of spontaneous excitatory transmission (Antonucci et al., 2012; Gabrielli et al., 2015; You et al., 2020) but upon chronic exposure EVs from reactive astrocytes exert detrimental effects on synapse stability (Prada et al., 2018), neurite differentiation and neuronal firing (You et al., 2020). Astrocyte-derived EVs isolated from plasma of AD patients carry high levels of complement effector proteins compared to healthy controls, suggesting that they could promote the spreading of inflammatory signals (Goetzl et al., 2018). By showing that TG2 sorted on the surface of astrocytic EVs has the capacity to regulate

neuronal Ca^{2+} homeostasis, we add an important piece of information to decipher the complex astrocyte-to-neuron signaling mediated by EVs under physiology and neuroinflammation.

The action of TG2 displayed in EVs, which are known to deliver concentrated factors to target cells (Turola et al., 2012), is reproduced by relatively high concentration of soluble extracellular TG2 (10-30 μg/ml), which may be reached under persistent astrocyte activation (Pinzon et al., 2017; Pinzon et al., 2019). TG2-dependent Ca^{2+} influx sets basal $[Ca^{2+}]_i$ at higher levels and promotes spontaneous EPSCs. This is a novel function that has never been attributed to TG2 before. Interestingly, $[Ca^{2+}]_i$ is restored to basal levels upon removal of TG2 from the extra-neuronal solution, revealing that the process is reversible and not linked to neuron damage. Reversibility of TG2 action suggests also that conformation rather than transamidating activity of the enzyme regulates $[Ca^{2+}]_i$ homeostasis, as covalent crosslinking of a substrate would lead to irreversible effects. Several past and present evidences suggest that TG2 is capable of crosslinking-independent modifications (Akimov et al., 2000; Stephens et al., 2004; Steppan et al., 2017; Verderio et al., 2003) and TG2 conformation is important in mediating the cellular response (Katt et al., 2018). In mouse striatal cells, TG2 in open conformation was shown to have cytotoxic effects, increasing the cells susceptibility to oxygen/glucose deprivation-mediated cell death. However, the underlying mechanism remains largely unknown (Colak et al., 2011; Singh et al., 2016).

Consistent with a crosslinking-independent role of TG2 in the control of Ca^{2+} dynamics, *in vitro* measurement of purified TG2 activity in KRH, mimicking the extracellular solution used for Ca^{2+} and electrophysiological recordings, showed that the protein is mostly inactive under this experimental condition. On the other hand, we cannot exclude that the enzyme transamidating activity may contribute, in part, to the control of neuronal Ca^{2+} homeostasis. For example, it could be hypothesized that residual TG2 activity may act on substrates present in the extracellular medium that could promote Ca^{2+} influx upon transamidation and which would be removed together with TG2 during the washing step, thus resulting in reversibility. In this respect, transamidation of monoamine neurotransmitters, a reaction called monoaminylation, is a less characterized function of TG2 that may play a role in the process (Muma, 2018). Therefore, further work is required to exclude the possible contribution of TG2 activity to the control of Ca^{2+} dynamics.

Importantly, we show that in physiological solution TG2 induces a small increase in neuronal $[Ca^{2+}]_i$, not associated to cell death, setting $[Ca^{2+}]_i$ to levels typically displayed by astrocytes in primary culture, that are significantly higher compared to neurons. Such increase in $[Ca^{2+}]_i$, is functionally relevant as it promotes neuronal

transmission (spontaneous EPSCs). This could suggest that in pathological conditions TG2 may also rescue defective transmission in damaged neurons, not only contributing to excitotoxicity and neuroinflammatory processes upon Ca^{2+} overload (Grosso & Mouradian, 2012).

Identification of L-type VOCCs and NCX as the TG2 molecular targets mediating Ca^{2+} influx and setting basal $[Ca^{2+}]_i$ at a higher levels in neurons, provides mechanistic understanding of the pathway. Both molecular targets have been identified using pharmacological blockers combined to Ca^{2+} and electrophysiological recordings. Interestingly, activation of L-type VOCCs is important for synaptic plasticity (Grover & Teyler, 1990; Raymond & Redman, 2002) such as long-term potentiation (LTP), suggesting that through this target TG2 may have a role in physiological brain functions. However, alterations in VOCCs activity have been also reported in neurodegeneration, such as in AD (LaFerla, 2002; Nimmrich & Eckert, 2013), suggesting that persistent activation of VOCCs may also contribute to degenerative processes. Similarly to VOCCs, NCX is fundamental for the regulation of $[Ca^{2+}]_i$ and activation of the reverse mode (Ca^{2+} influx) has been associated with neuropathic pain caused by nerve-injury (Jaggi & Singh, 2011), ischemic damage (Matsuda et al., 2001), increased oxygen/glucose deprivation-mediated neuronal damage and infarct injury (Secondo et al., 2015). Thus, sustained elevations of TG2 in the extracellular environment, via NCX reverse operation and opening of L-type VOCCs, could participate to general dysregulation of Ca^{2+} homeostasis in neurodegenerative conditions. Analysis of the TG2 interactome has identified a subunit of Na^+/K^+-transporting ATPase as partner of extracellular TG2, and our data suggest that its inhibition by TG2 could reverse the activity of NCX, thus leading to Ca^{2+} inward flux and the opening of L-type VOCCs.

5. Conclusions

In conclusion, our data highlight for the first time a specific function of extracellular TG2, either released by astrocytes via EVs or in soluble form, on Ca^{2+} homeostasis in neurons, through NCX operation in the reverse mode and opening of L-type VOCCs, likely mediated by the Na^+/K^+-transporting ATPase (Fig. 9). This is the first evidence that astrocytes control intraneuronal Ca^{2+} through release of TG2 in association with EVs.

Acknowledgments

We are grateful to Prof Jeff Keillor (University of Ottawa, Canada) for critically reading the manuscript. We thank Prof David Abraham (University College London/Medical School, United Kingdom) and Prof Timothy Johnson (University of Sheffield, United Kingdom) for generously sharing facilities. We are grateful to Dr Giulia D'Arrigo (CNR Institute of Neuroscience, Italy) for her help in maintaining the primary cell cultures and we gratefully acknowledge the NTU Imaging Suite and Dr Graham J. Hickman for assistance in obtaining TEM data.

Funding:

This work was supported by the John Turland PhD scholarship (to E.T. and E.A.M.V.), the American Association Research fellowship (to I.P. and C.V.) (grant number AARF-588984), the IBRO/PERC InEurope Short Stay grant to E.T, the AIRC fellowship for Italy to I.V., The Marmont Foundation and the Nottingham Trent University REF-Quality Research fund (to E.A.M.V.).

Author Contribution Statement

E.T., M.M, C.V. and E.A.M.V conceived and designed research. E.T., I.V., M.G., G.F., C.C. and M.P.S performed research. E.T., I.V., I.P., M.G., D.J.B., G.S., M.M., C.V. and E.A.M.V analyzed and interpreted data. E.T., I.V., C.V. and E.A.M.V. wrote the paper. All authors read and approved the final paper.

Conflict of Interest Statement

The authors declare that they have no conflict of interest.

Data Availability Statement

The mass spectrometry proteomics datasets have been deposited to the ProteomeXchange Consortium via the PRIDE (Perez-Riverol et al., 2019) partner repository with the dataset identifier "PXD022224" (http://www.ebi.ac.uk/pride). The rest of the data are included in this published article (and its supplementary information files).

References

Akimov, S.S., Krylov, D., Fleischman, L.F., Belkin, A.M. (2000). Tissue transglutaminase is an integrin-binding adhesion coreceptor for fibronectin. J Cell Biol 148, 825-38. https://10.1083/jcb.148.4.825

Andringa, G., Lam, K.Y., Chegary, M., Wang, X., Chase, T.N., Bennett, M.C. (2004). Tissue transglutaminase catalyzes the formation of alpha-synuclein crosslinks in Parkinson's disease. FASEB J 18, 932-4. https://10.1096/fj.03-0829fje

Antonucci, F., Turola, E., Riganti, L., Caleo, M., Gabrielli, M., Perrotta, C., Novellino, L., Clementi, E., Giussani, P., Viani, P., Matteoli, M., Verderio, C. (2012). Microvesicles released from microglia stimulate synaptic activity via enhanced sphingolipid metabolism. EMBO J 31, 1231-40. https://10.1038/emboj.2011.489

Antonyak, M.A., Li, B., Boroughs, L.K., Johnson, J.L., Druso, J.E., Bryant, K.L., Holowka, D.A., Cerione, R.A. (2011). Cancer cell-derived microvesicles induce transformation by transferring tissue transglutaminase and fibronectin to recipient cells. Proc Natl Acad Sci U S A 108, 4852-7. https://10.1073/pnas.1017667108

Bacci, A., Verderio, C., Pravettoni, E., Matteoli, M. (1999). Synaptic and intrinsic mechanisms shape synchronous oscillations in hippocampal neurons in culture. Eur J Neurosci 11, 389-97. https://10.1046/j.1460-9568.1999.00440.x

Benilova, I., Karran, E., De Strooper, B. (2012). The toxic Abeta oligomer and Alzheimer's disease: an emperor in need of clothes. Nat Neurosci 15, 349-57. https://10.1038/nn.3028

Blaustein, M.P., Lederer, W.J. (1999). Sodium/calcium exchange: its physiological implications. Physiol Rev 79, 763-854. https://10.1152/physrev.1999.79.3.763

Carafoli, E. (1987). Intracellular calcium homeostasis. Annu Rev Biochem 56, 395-433. https://10.1146/annurev.bi.56.070187.002143

Catterall, W.A., Few, A.P. (2008). Calcium channel regulation and presynaptic plasticity. Neuron 59, 882-901. https://10.1016/j.neuron.2008.09.005

Charrin, S., Palmulli, R., Billard, M., Clay, D., Boucheix, C., Van Niel, G., Rubinstein, E. (2020). Rapid Isolation of Rare Isotype-Switched Hybridoma Variants: Application to the Generation of IgG2a and IgG2b MAb to CD63, a Late Endosome and Exosome Marker. Antibodies (Basel) 9https://10.3390/antib9030029

Chen, X.D., Zhao, J., Yan, Z., Zhou, B.W., Huang, W.F., Liu, W.F., Li, C., Liu, K.X. (2020). Isolation of extracellular vesicles from intestinal tissue in a mouse model of intestinal ischemia/reperfusion injury. Biotechniques 68, 257-262. https://10.2144/btn-2019-0159

Colak, G., Johnson, G.V. (2012). Complete transglutaminase 2 ablation results in reduced stroke volumes and astrocytes that exhibit increased survival in response to ischemia. Neurobiol Dis 45, 1042-50. https://10.1016/j.nbd.2011.12.023

Colak, G., Keillor, J.W., Johnson, G.V. (2011). Cytosolic guanine nucledotide binding deficient form of transglutaminase 2 (R580a) potentiates cell death in oxygen glucose deprivation. PLoS One 6, e16665. https://10.1371/journal.pone.0016665

Colombo, E., Farina, C. (2016). Astrocytes: Key Regulators of Neuroinflammation. Trends Immunol 37, 608-620. https://10.1016/j.it.2016.06.006

Condliffe, S.B., Corradini, I., Pozzi, D., Verderio, C., Matteoli, M. (2010). Endogenous SNAP-25 regulates native voltage-gated calcium channels in glutamatergic neurons. J Biol Chem 285, 24968-76. https://10.1074/jbc.M110.145813

D'Arrigo, G., Gabrielli, M., Scaroni, F., Swuec, P., Amin, L., Pegoraro, A., Adinolfi, E., Di Virgilio, F., Cojoc, D., Legname, G., Verderio, C. (2021). Astrocytes-derived extracellular vesicles in motion at the neuron surface: Involvement of the prion protein. J Extracell Vesicles 10, e12114. https://10.1002/jev2.12114

De Laurenzi, V., Melino, G. (2001). Gene disruption of tissue transglutaminase. Mol Cell Biol 21, 148-55. https://10.1128/MCB.21.1.148-155.2001

Diaz-Hidalgo, L., Altuntas, S., Rossin, F., D'Eletto, M., Marsella, C., Farrace, M.G., Falasca, L., Antonioli, M., Fimia, G.M., Piacentini, M. (2016). Transglutaminase type 2-dependent selective recruitment of proteins into exosomes under stressful cellular conditions. Biochim Biophys Acta 1863, 2084-92. https://10.1016/j.bbamcr.2016.05.005

Dunkley, P.R., Jarvie, P.E., Robinson, P.J. (2008). A rapid Percoll gradient procedure for preparation of synaptosomes. Nat Protoc 3, 1718-28. https://10.1038/nprot.2008.171

Farhy-Tselnicker, I., Allen, N.J. (2018). Astrocytes, neurons, synapses: a tripartite view on cortical circuit development. Neural Dev 13, 7. https://10.1186/s13064-018-0104-y

Feola, J., Barton, A., Akbar, A., Keillor, J., Johnson, G.V.W. (2017). Transglutaminase 2 modulation of NF-kappaB signaling in astrocytes is independent of its ability to mediate astrocytic viability in ischemic injury. Brain Res 1668, 1-11. https://10.1016/j.brainres.2017.05.009

Forti, L., Pouzat, C., Llano, I. (2000). Action potential-evoked Ca2+ signals and calcium channels in axons of developing rat cerebellar interneurones. J Physiol 527 Pt 1, 33-48. https://10.1111/j.1469-7793.2000.00033.x

Furini, G., Schroeder, N., Huang, L., Boocock, D., Scarpellini, A., Coveney, C., Tonoli, E., Ramaswamy, R., Ball, G., Verderio, C., Johnson, T.S., Verderio, E.A.M. (2018). Proteomic Profiling Reveals the Transglutaminase-2 Externalization Pathway in Kidneys after Unilateral Ureteric Obstruction. J Am Soc Nephrol 29, 880-905. https://10.1681/ASN.2017050479

Gable, M.E., Ellis, L., Fedorova, O.V., Bagrov, A.Y., Askari, A. (2017). Comparison of Digitalis Sensitivities of Na(+)/K(+)-ATPases from Human and Pig Kidneys. ACS Omega 2, 3610-3615. https://10.1021/acsomega.7b00591

Gabrielli, M., Battista, N., Riganti, L., Prada, I., Antonucci, F., Cantone, L., Matteoli, M., Maccarrone, M., Verderio, C. (2015). Active endocannabinoids are secreted on extracellular membrane vesicles. EMBO Rep 16, 213-20. https://10.15252/embr.201439668

Goetzl, E.J., Schwartz, J.B., Abner, E.L., Jicha, G.A., Kapogiannis, D. (2018). High complement levels in astrocyte-derived exosomes of Alzheimer disease. Ann Neurol 83, 544-552. https://10.1002/ana.25172

Greotti, E., Capitanio, P., Wong, A., Pozzan, T., Pizzo, P., Pendin, D. (2019). Familial Alzheimer's disease-linked presenilin mutants and intracellular Ca(2+) handling: A single-organelle, FRET-based analysis. Cell Calcium 79, 44-56. https://10.1016/j.ceca.2019.02.005

Grosso, H., Mouradian, M.M. (2012). Transglutaminase 2: biology, relevance to neurodegenerative diseases and therapeutic implications. Pharmacol Ther 133, 392-410. https://10.1016/j.pharmthera.2011.12.003

Grosso, H., Woo, J.M., Lee, K.W., Im, J.Y., Masliah, E., Junn, E., Mouradian, M.M. (2014). Transglutaminase 2 exacerbates alpha-synuclein toxicity in mice and yeast. FASEB J 28, 4280-91. https://10.1096/fj.14-251413

Grover, L.M., Teyler, T.J. (1990). Two components of long-term potentiation induced by different patterns of afferent activation. Nature 347, 477-9. https://10.1038/347477a0

Hartley, D.M., Zhao, C., Speier, A.C., Woodard, G.A., Li, S., Li, Z., Walz, T. (2008). Transglutaminase induces protofibril-like amyloid beta-protein assemblies that are protease-resistant and inhibit long-term potentiation. J Biol Chem 283, 16790-800. https://10.1074/jbc.M802215200

Holm, M.M., Kaiser, J., Schwab, M.E. (2018). Extracellular Vesicles: Multimodal Envoys in Neural Maintenance and Repair. Trends Neurosci 41, 360-372. https://10.1016/j.tins.2018.03.006

Hostenbach, S., Cambron, M., D'Haeseleer, M., Kooijman, R., De Keyser, J. (2014). Astrocyte loss and astrogliosis in neuroinflammatory disorders. Neurosci Lett 565, 39-41. https://10.1016/j.neulet.2013.10.012

Ientile, R., Curro, M., Caccamo, D. (2015). Transglutaminase 2 and neuroinflammation. Amino Acids 47, 19-26. https://10.1007/s00726-014-1864-2

Jaggi, A.S., Singh, N. (2011). Therapeutic targets for the management of peripheral nerve injury-induced neuropathic pain. CNS Neurol Disord Drug Targets 10, 589-609. https://10.2174/187152711796235041

Jones, H.C., Keep, R.F. (1988). Brain fluid calcium concentration and response to acute hypercalcaemia during development in the rat. J Physiol 402, 579-93. https://10.1113/jphysiol.1988.sp017223

Joshi, P., Turola, E., Ruiz, A., Bergami, A., Libera, D.D., Benussi, L., Giussani, P., Magnani, G., Comi, G., Legname, G., Ghidoni, R., Furlan, R., Matteoli, M., Verderio, C. (2014). Microglia convert aggregated amyloid-beta into neurotoxic forms through the shedding of microvesicles. Cell Death Differ 21, 582-93. https://10.1038/cdd.2013.180

Junn, E., Ronchetti, R.D., Quezado, M.M., Kim, S.Y., Mouradian, M.M. (2003). Tissue transglutaminase-induced aggregation of alpha-synuclein: Implications for Lewy body formation in Parkinson's disease and dementia with Lewy bodies. Proc Natl Acad Sci U S A 100, 2047-52. https://10.1073/pnas.0438021100

Katt, W.P., Antonyak, M.A., Cerione, R.A. (2018). Opening up about Tissue Transglutaminase: When Conformation Matters More than Enzymatic Activity. Med One 3https://10.20900/mo.20180011

LaFerla, F.M. (2002). Calcium dyshomeostasis and intracellular signalling in Alzheimer's disease. Nat Rev Neurosci 3, 862-72. https://10.1038/nrn960

Leitch, B., Szostek, A., Lin, R., Shevtsova, O. (2009). Subcellular distribution of L-type calcium channel subtypes in rat hippocampal neurons. Neuroscience 164, 641-57. https://10.1016/j.neuroscience.2009.08.006

Marambaud, P., Dreses-Werringloer, U., Vingtdeux, V. (2009). Calcium signaling in neurodegeneration. Mol Neurodegener 4, 20. https://10.1186/1750-1326-4-20

Matsuda, T., Arakawa, N., Takuma, K., Kishida, Y., Kawasaki, Y., Sakaue, M., Takahashi, K., Takahashi, T., Suzuki, T., Ota, T., Hamano-Takahashi, A., Onishi, M., Tanaka, Y., Kameo, K., Baba, A. (2001). SEA0400, a novel and selective inhibitor of the Na+-Ca2+ exchanger, attenuates reperfusion injury in the in vitro and in vivo cerebral ischemic models. J Pharmacol Exp Ther 298, 249-56.

Monteagudo, A., Feola, J., Natola, H., Ji, C., Proschel, C., Johnson, G.V.W. (2018). Depletion of astrocytic transglutaminase 2 improves injury outcomes. Mol Cell Neurosci 92, 128-136. https://10.1016/j.mcn.2018.06.007

Muma, N.A. (2018). Transglutaminase in Receptor and Neurotransmitter-Regulated Functions. Med One 3https://10.20900/mo.20180012

Nikoletopoulou, V., Tavernarakis, N. (2012). Calcium homeostasis in aging neurons. Front Genet 3, 200. https://10.3389/fgene.2012.00200

Nimmrich, V., Eckert, A. (2013). Calcium channel blockers and dementia. Br J Pharmacol 169, 1203-10. https://10.1111/bph.12240

Oh, M.M., Oliveira, F.A., Waters, J., Disterhoft, J.F. (2013). Altered calcium metabolism in aging CA1 hippocampal pyramidal neurons. J Neurosci 33, 7905-11. https://10.1523/JNEUROSCI.5457-12.2013

Pan, S., Wang, R., Zhou, X., Corvera, J., Kloc, M., Sifers, R., Gallick, G.E., Lin, S.H., Kuang, J. (2008). Extracellular Alix regulates integrin-mediated cell adhesions and extracellular matrix assembly. EMBO J 27, 2077-90. https://10.1038/emboj.2008.134

Papouin, T., Dunphy, J., Tolman, M., Foley, J.C., Haydon, P.G. (2017). Astrocytic control of synaptic function. Philos Trans R Soc Lond B Biol Sci 372https://10.1098/rstb.2016.0154

Perez-Riverol, Y., Csordas, A., Bai, J., Bernal-Llinares, M., Hewapathirana, S., Kundu, D.J., Inuganti, A., Griss, J., Mayer, G., Eisenacher, M., Perez, E., Uszkoreit, J., Pfeuffer, J., Sachsenberg, T., Yilmaz, S., Tiwary, S., Cox, J., Audain, E., Walzer, M., Jarnuczak, A.F. et al. (2019). The PRIDE database and related tools and resources in 2019: improving support for quantification data. Nucleic Acids Res 47, D442-D450. https://10.1093/nar/gky1106

Pinzon, N.E., Breve, J.J.P., Bol, J., Drukarch, B., Baron, W., van Dam, A.M. (2017). Tissue transglutaminase in astrocytes is enhanced by inflammatory mediators and is involved in the formation of fibronectin fibril-like structures. J Neuroinflammation 14, 260. https://10.1186/s12974-017-1031-2

Pinzon, N.E., van Mierlo, H., de Jonge, J.C., Breve, J.J.P., Bol, J., Drukarch, B., van Dam, A.M., Baron, W. (2019). Tissue Transglutaminase Promotes Early Differentiation of Oligodendrocyte Progenitor Cells. Front Cell Neurosci 13, 281. https://10.3389/fncel.2019.00281

Prada, I., Gabrielli, M., Turola, E., Iorio, A., D'Arrigo, G., Parolisi, R., De Luca, M., Pacifici, M., Bastoni, M., Lombardi, M., Legname, G., Cojoc, D., Buffo, A., Furlan, R., Peruzzi, F., Verderio, C. (2018). Glia-to-neuron transfer of miRNAs via extracellular vesicles: a new mechanism underlying inflammation-induced synaptic alterations. Acta Neuropathol 135, 529-550. https://10.1007/s00401-017-1803-x

Pravettoni, E., Bacci, A., Coco, S., Forbicini, P., Matteoli, M., Verderio, C. (2000). Different localizations and functions of L-type and N-type calcium channels during development of hippocampal neurons. Dev Biol 227, 581-94. https://10.1006/dbio.2000.9872

Quinn, B.R., Yunes-Medina, L., Johnson, G.V.W. (2018). Transglutaminase 2: Friend or foe? The discordant role in neurons and astrocytes. J Neurosci Res 96, 1150-1158. https://10.1002/jnr.24239

Raymond, C.R., Redman, S.J. (2002). Different calcium sources are narrowly tuned to the induction of different forms of LTP. J Neurophysiol 88, 249-55. https://10.1152/jn.2002.88.1.249

Scarpellini, A., Huang, L., Burhan, I., Schroeder, N., Funck, M., Johnson, T.S., Verderio, E.A. (2014). Syndecan-4 knockout leads to reduced extracellular transglutaminase-2 and protects against tubulointerstitial fibrosis. J Am Soc Nephrol 25, 1013-27. https://10.1681/ASN.2013050563

Secondo, A., Pignataro, G., Ambrosino, P., Pannaccione, A., Molinaro, P., Boscia, F., Cantile, M., Cuomo, O., Esposito, A., Sisalli, M.J., Scorziello, A., Guida, N., Anzilotti, S., Fiorino, F., Severino, B., Santagada, V., Caliendo, G., Di Renzo, G., Annunziato, L. (2015). Pharmacological characterization of the newly synthesized 5-amino-N-butyl-2-(4-ethoxyphenoxy)-benzamide hydrochloride (BED) as a potent NCX3 inhibitor that worsens anoxic injury in cortical neurons, organotypic hippocampal cultures, and ischemic brain. ACS Chem Neurosci 6, 1361-70. https://10.1021/acschemneuro.5b00043

Singh, G., Zhang, J., Ma, Y., Cerione, R.A., Antonyak, M.A. (2016). The Different Conformational States of Tissue Transglutaminase Have Opposing Affects on Cell Viability. J Biol Chem 291, 9119-32. https://10.1074/jbc.M115.699108

Slot, J.W., Geuze, H.J. (2007). Cryosectioning and immunolabeling. Nat Protoc 2, 2480-91. https://10.1038/nprot.2007.365

Stellwagen, D., Malenka, R.C. (2006). Synaptic scaling mediated by glial TNF-alpha. Nature 440, 1054-9. https://10.1038/nature04671

Stephens, P., Grenard, P., Aeschlimann, P., Langley, M., Blain, E., Errington, R., Kipling, D., Thomas, D., Aeschlimann, D. (2004). Crosslinking and G-protein functions of transglutaminase 2 contribute differentially to fibroblast wound healing responses. J Cell Sci 117, 3389-403. https://10.1242/jcs.01188

Steppan, J., Bergman, Y., Viegas, K., Armstrong, D., Tan, S., Wang, H., Melucci, S., Hori, D., Park, S.Y., Barreto, S.F., Isak, A., Jandu, S., Flavahan, N., Butlin, M., An, S.S., Avolio, A., Berkowitz, D.E., Halushka, M.K., Santhanam, L. (2017). Tissue Transglutaminase Modulates Vascular Stiffness and Function Through Crosslinking-Dependent and Crosslinking-Independent Functions. J Am Heart Assoc 6https://10.1161/JAHA.116.004161

Tucholski, J., Roth, K.A., Johnson, G.V. (2006). Tissue transglutaminase overexpression in the brain potentiates calcium-induced hippocampal damage. J Neurochem 97, 582-94. https://10.1111/j.1471-4159.2006.03780.x

Turola, E., Furlan, R., Bianco, F., Matteoli, M., Verderio, C. (2012). Microglial microvesicle secretion and intercellular signaling. Front Physiol 3, 149. https://10.3389/fphys.2012.00149

Verderio, C., Bacci, A., Coco, S., Pravettoni, E., Fumagalli, G., Matteoli, M. (1999). Astrocytes are required for the oscillatory activity in cultured hippocampal neurons. Eur J Neurosci 11, 2793-800. https://10.1046/j.1460-9568.1999.00697.x

Verderio, E., Nicholas, B., Gross, S., Griffin, M. (1998). Regulated expression of tissue transglutaminase in Swiss 3T3 fibroblasts: effects on the processing of fibronectin, cell attachment, and cell death. Exp Cell Res 239, 119-38. https://10.1006/excr.1997.3874

Verderio, E.A., Furini, G., Burhan, I.W., Johnson, T.S. (2015). Transglutaminases: Expression in kidney and relation to kidney fibrosis. In *Transglutaminases* Hitomi K, Kojima S, Fesus L (eds) pp 229-262. Springer Japan.

Verderio, E.A., Telci, D., Okoye, A., Melino, G., Griffin, M. (2003). A novel RGD-independent cel adhesion pathway mediated by fibronectin-bound tissue transglutaminase rescues cells from anoikis. J Biol Chem 278, 42604-14. https://10.1074/jbc.M303303200

You, Y., Borgmann, K., Edara, V.V., Stacy, S., Ghorpade, A., Ikezu, T. (2020). Activated human astrocyte-derived extracellular vesicles modulate neuronal uptake, differentiation and firing. J Extracell Vesicles 9, 1706801. https://10.1080/20013078.2019.1706801

Figure legends

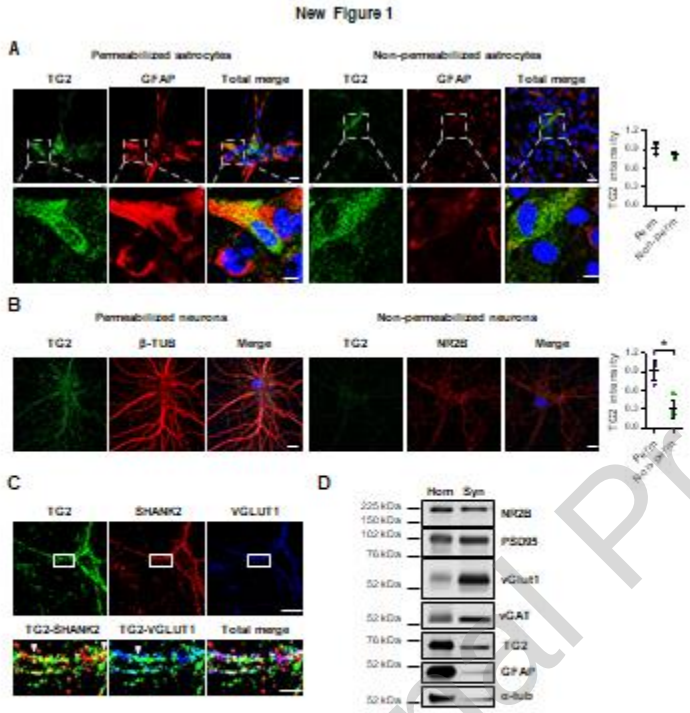

Figure 1. TG2 localizes extracellularly in primary astrocytes and at synaptic sites in neurons.

(A) Immunofluorescence staining of primary astrocytes. Cells were fixed in 4% paraformaldehyde - 4 % sucrose (w/v), permeabilized (left panels) or non-permeabilized (right panel) and stained with anti-TG2 IA12 (green), DAPI (blue) and astrocytic marker anti-GFAP (red). Coverslips were visualized by laser scanning Leica SP5 confocal microscope using 63X oil immersion objective. Successive serial optical sections (1 µm) were recorded over 8 µm planes. Scale bar 20 µm. TG2 intensity was calculated by Leica software, divided by number of nuclei, and normalized to permeabilized values. Data is expressed as mean ± SD (N=3, Mann-Whitney test: p=NS).

(B) Neurons at 12 DIV were fixed and permeabilized (left panel) or non-permeabilized (right panel) and stained with anti-TG2 IA12 (green), anti-β-TUB or anti-NR2B (red) antibodies and DAPI (blue). Scale bar 10 µm. TG2 intensity was calculated as described in A (N=3, Mann-Whitney test: *p<0.05).

(C) Neurons at 22 Days In Vitro (DIV) were fixed, permeabilized and stained with anti-TG2 IA12 (green), anti-SHANK2 (red) and anti-VGLUT1 (blue) antibodies (N=3). Coverslips were visualized as described in A. Scale bar 20 µm (low magnification) and 5 µm (high magnification).

(D) Synaptosomes were isolated from adult mouse brain and probed with pre- and post-synaptic markers and for astrocyte marker GFAP. α-tubulin was used as loading control. TG2 is present in the synaptic fraction (Syn) as well as the total brain homogenate (Hom).

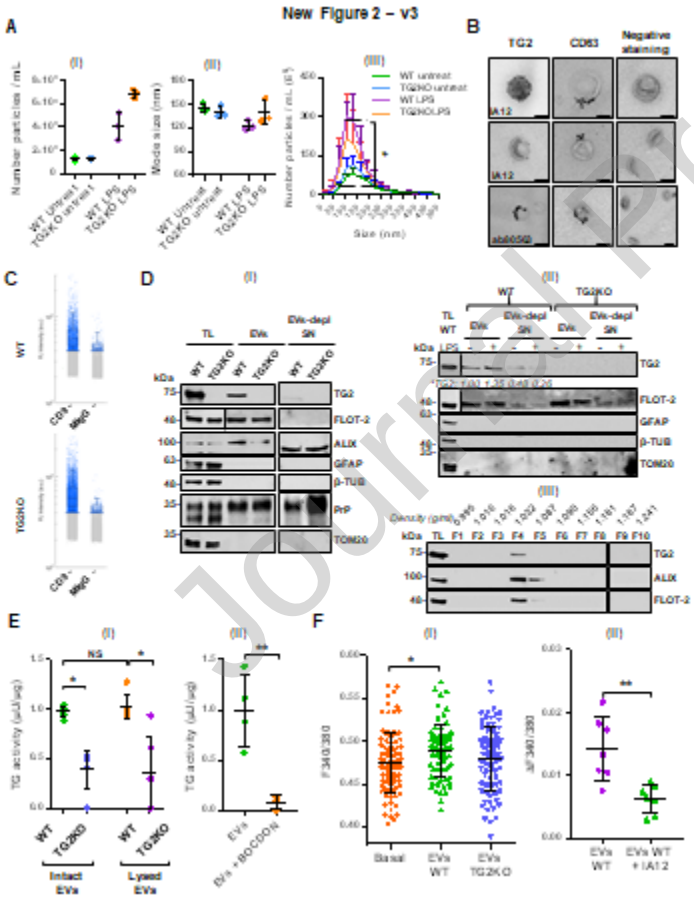

Figure 2. Astrocytic TG2 is released in association with EVs and modulates calcium homeostasis in neurons.

(A) EVs characterization by nanoparticle tracking analysis (NTA). Average particle concentration (I) and mode size (II) of EVs isolated from untreated and LPS-treated WT and TG2KO astrocytes characterized by NTA (ZetaView, Particle Metrix). Data is shown as mean ± SD (N=3 independent experiments, Kruskal-Wallis Dunn's test: p=NS). (III) Graph showing average particle concentration according to EVs size (Kruskal-Wallis Dunn's test WT untreated – WT LPS: *p<0.05).

(B) EVs characterization by Transmission electron microscopy (TEM). TEM analysis of EVs isolated from untreated WT astrocytes and stained with either anti-CD63 antibody (Abcam) or anti-TG2 antibody (monoclonal IA12 and polyclonal ab80653) and 6 nm gold colloidal anti-mouse IgG or 18 nm gold colloidal anti-rabbit IgG, or negative stained with uranyl acetate methylcellulose.

C) Characterization of EVs by ExoView R200 platform. Plots show fluorescence intensity (average of 3 spots ± SD) of single EV particles (WT or TG2KO) immunocaptured with CD9 antibody or control IgG.

(D) Western blotting analysis of astrocytes-derived EVs and proteins TCA-precipitated from 10 ml of vesicle-depleted supernatants (EVs-depl SN) for the detection of EVs markers ALIX, FLOT-2 and PrP, EVs negative marker TOM20, glial marker GFAP and of TG2. β-tubulin was used as loading control for TL. (I) Conditioned medium was centrifuged at 200,000xg for 3 h and EVs-depleted SN filtered prior to TCA precipitation. All pelleted proteins were loaded (WT SN: 70 µg; TG2KO SN: 100 µg). (II) Conditioned medium was centrifuged at 110,000xg for 70 min as per standard procedure. A representative blot of 3 independent experiments is shown. Treated cells were primed with LPS (1 µg/ml) for 24 h in serum-free medium before EVs isolation. Vertical black lines separate sections of the same membrane developed for different exposition times. * Densitometry quantification of TG2 is shown (N=2). (III) EVs pellets, obtained by standard ultracentrifugation, were processed by density gradient ultracentrifugation (Optiprep) as described in the Methods. The ten collected fractions (F) were analysed by western blotting for the detection of TG2, ALIX and FLOT-2.

(E) (I) Comparison of TG2 activity in intact and lysed EVs isolated from WT and TG2KO astrocytes. EVs were either resuspended as intact in PBS or lysed in a mild sucrose buffer, to detect surface TG2 activity or total activity respectively. Data are expressed as mean ± SD normalized to WT intact and lysed EVs values respectively (N=3 independent experiments; Kruskal-Wallis Dunn's test: *p<0.05. Intact WT EVs: 7.3±3.6 nU/µg; lysed WT EVs: 4.7±2.6 nU/µg; p=NS). (II) Intact EVs were analyzed in the presence or absence of non-permeable

TG2 inhibitor BOCDON. Data are expressed as mean ± SD normalized to untreated EVs (N=2 independent experiments; Student's t-test: **p<0.01).

(F) (I) Quantification of $[Ca^{2+}]_i$, expressed as F340/380, in 13 DIV neurons before and after stimulation with similar levels of EVs (estimated µg: WT EVs+LPS = 12.2±2.3; TG2KO EVs+LPS = 15.9±6.6) isolated from LPS-treated WT or TG2KO astrocytes (N≥75 neurons from a preparation derived from ≥10 rat E18 embryos). EVs from either WT or TG2KO cells were resuspended in KRH supplemented with 30 U/ml of apyrase and added to neurons in the presence of 1 µM TTX, 50 µM APV and 10 µM CNQX. $[Ca^{2+}]_i$ was measured in multiple fields before (basal) and 20-60 min after addition of either WT or TG2KO EVs. Data are expressed as mean ± SD (one-way ANOVA test: *p<0.05). The level of TG2 displayed by astrocytic EVs was about 5 µg/ml (indirectly calculated by activity assay). (II) Quantification of $[Ca^{2+}]_i$, changes in neurons (N=7 neurons), expressed as ΔF340/380, after stimulation with WT EVs pre-treated or not with mouse monoclonal antibody IA12. Data are expressed as mean ± SD (Mann-Whitney test: **p<0.01).

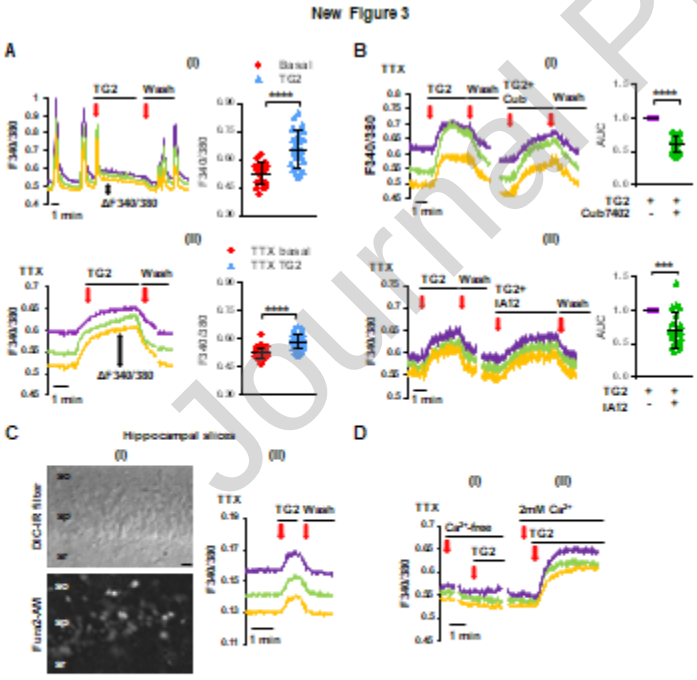

Figure 3. Exogenous TG2 increases interspike and basal $[Ca^{2+}]_i$ in hippocampal neurons in culture and in brain slices.

(A) (I) Representative temporal analysis of synchronous Ca^{2+} oscillations, expressed as F340/380, spontaneously occurring in 14 DIV Fura-2-loaded hippocampal neurons. Addition of exogenous TG2 (10 µg/ml) promoted a Ca^{2+} spike followed by a sustained Ca^{2+} plateau (indicated by ΔF340/380), with a block of oscillations. Upon TG2 removal (wash with KRH) synchronous Ca^{2+} oscillations re-started. Three representative traces of neuronal $[Ca^{2+}]_i$ are shown in each graph. The graph shows the quantification of TG2-induced interspike $[Ca^{2+}]_i$ elevations compared with basal $[Ca^{2+}]_i$ (N=23 neurons, Student's t-test: ****p<0.0001). (II) Addition of exogenous TG2 (10 µg/ml) in the presence of TTX (1 µM) significantly increased $[Ca^{2+}]_i$ (indicated by ΔF340/380). Graph shows the quantification of TG2-induced $[Ca^{2+}]_i$ rises (peak Ca^{2+} rise) compared with basal $[Ca^{2+}]_i$ in the presence of TTX (N=33 neurons, Student's t-test: ****p<0.0001). Data are presented as mean F340/380 ± SD.

(B) Temporal analysis of $[Ca^{2+}]_i$ changes induced by TG2 in the presence of mouse monoclonal anti-TG2 antibodies CUB7402 and IA12. (I) Total Ca^{2+} influxes in response to TG2 were reduced of about 40% in mouse hippocampal neurons when TG2 was pre-incubated with CUB7402 antibody (1:150 dilution). Data are expressed as mean AUC ± SD induced by TG2+CUB7402 normalized to TG2 alone (N=25 neurons; Wilcoxon signed-rank test: ****p<0.0001). (II) Total Ca^{2+} influxes in response to TG2 were reduced of about 30% when TG2 was pre-incubated with IA12 antibody (1:150 dilution). Data are expressed as mean AUC ± SD induced by TG2+IA12 normalized to TG2 alone (N=21 neurons; Wilcoxon signed-rank test: ***p<0.001)

(C) (I) Representative DIC (top) and 380 nm fluorescence (bottom) images of neurons in the stratum pyramidale (sp) of mouse hippocampal slices loaded with Fura-2/AM for calcium imaging experiments. The stratum oriens (so) and stratum radiatum (sr) are indicated above and below sp respectively. (II) Representative temporal plot of $[Ca^{2+}]_i$ rises evoked by perfusion of extracellular TG2 in fura-2 loaded hippocampal slices in 1 µM TTX (N=3 brain slices, 28 neurons in total).

(D) Temporal analysis of $[Ca^{2+}]_i$ changes in 14-20 DIV neurons exposed to exogenous TG2 in the absence (I) or in the presence (II) of extracellular Ca^{2+}. Addition of TG2 in the absence of extracellular Ca^{2+} did not lead to changes in $[Ca^{2+}]_i$ (N=31 neurons).

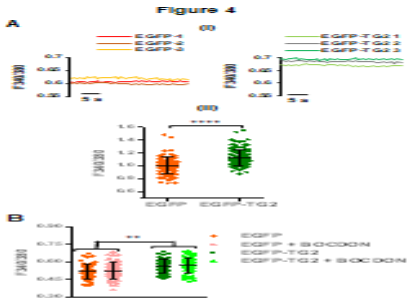

Figure 4. Transfected TG2 induces a calcium rise in an autocrine manner in neurons.

(A) (I) Representative traces showing basal $[Ca^{2+}]_i$, expressed as F340/380, in pEGFP-N1-TG2 or pEGFP-N1 transfected neurons (8 DIV). (II) Graph showing $[Ca^{2+}]_i$, in transfected neurons expressed as mean F340/380 ± SD normalized to EGFP (N>100 neurons. Mann-Whitney test: ****p<0.0001).

(B) A subgroup of transfected neurons was treated with the non-permeable TG2 inhibitor BOCDON (200 µM), which did not affect $[Ca^{2+}]_i$ (N>45 neurons). A significant difference in $[Ca^{2+}]_i$ between EGFP and EGFP-TG2 was observed in this subgroup as in graph A-II (one-way ANOVA test: **p<0.01).

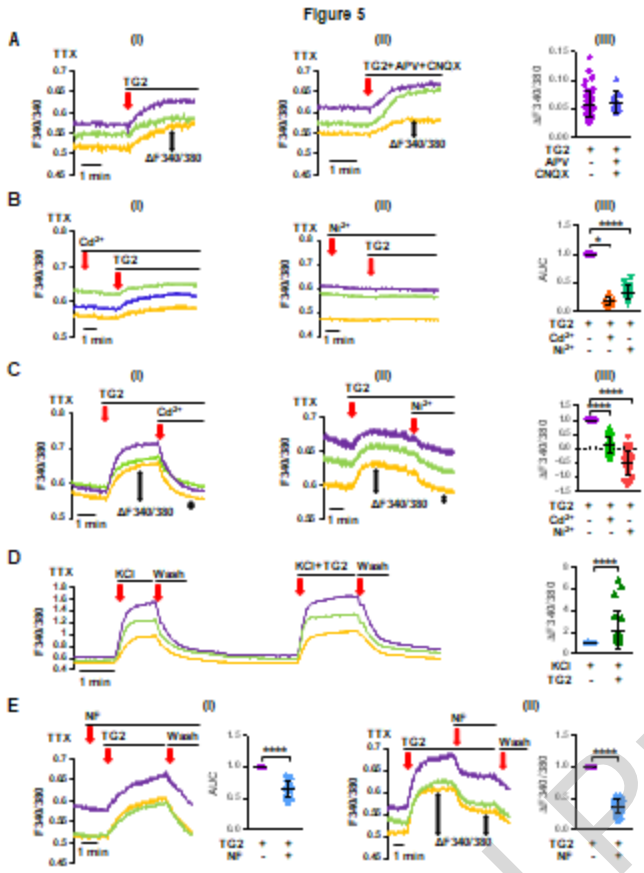

Figure 5. Exogenous TG2 mediates Ca^{2+} influx from the extracellular environment.

(A) Temporal analysis of $[Ca^{2+}]_i$ changes in 14-20 DIV neurons exposed to exogenous TG2 in the absence (I) or in the presence (II) of APV (NMDA receptor antagonist) and CNQX (AMPA/kainate receptor antagonist). TG2-dependent Ca^{2+} rise was not affected by the blockers. (III) Corresponding quantification of TG2-induced peak $[Ca^{2+}]_i$ rises. Data are presented as mean ΔF340/380 ± SD (N=46 and 9 neurons for TG2 alone and TG2+blockers respectively; Mann-Whitney test: p=NS).

(B) Pre-treatment with cadmium (I), a general blocker of Ca^{2+} channels, and nickel (II), a blocker of T-type VOCCs, reduced TG2-dependent Ca^{2+} responses of about 82.4% and 66.2% respectively, as quantified in (III), by measuring total Ca^{2+} influxes. Data are expressed as mean area under the curve (AUC) ± SD of TG2 + blockers normalized to TG2 alone (N=7 and 15 neurons for treatment with Cd^{2+} and Ni^{2+} respectively Wilcoxon signed-rank test: *p<0.05; ****p<0.0001).

(C) Addition of cadmium (I) and nickel (II) during the plateau phase of TG2-induced Ca^{2+} response led to a recovery of $[Ca^{2+}]_i$ towards basal levels. (III) Histograms show residual mean Ca^{2+} responses after blockers

normalized to peak Ca^{2+} response evoked by TG2 ± SD (N=18 and 25 neurons for treatment with Cd^{2+} and Ni^{2+} respectively; Wilcoxon signed-rank test: ****p<0.0001).

(D) Ca^{2+} transients induced by 15 mM KCl in the presence of NMDAR and ampa/kainate receptor blockers APV and CNQX revealed that $[Ca^{2+}]_i$ rose faster and led to a 2-fold higher total Ca^{2+} influx in the presence of TG2. Data are expressed as mean AUC of TG2 + KCl normalized to KCl alone treatment ± SD (N=22 neurons; Wilcoxon signed-rank test: ****p<0.0001).

(E) Temporal analysis of $[Ca^{2+}]_i$ changes induced by TG2 in the presence of L-type VOCCs blocker Nifedipine (NF). (I) Total Ca^{2+} influxes in response to TG2 were reduced of about 36% in neurons pre-treated with NF. Data are expressed as mean AUC ± SD induced by TG2 in the presence of NF normalized to TG2 alone (N=21 neurons; Wilcoxon signed-rank test: ****p<0.0001). (II) NF caused a partial recovery of about 63% of Ca^{2+} concentration towards resting levels when applied during the plateau phase of Ca^{2+} response induced by exogenous TG2. Histograms show mean residual Ca^{2+} responses ± SD after NF normalized to peak Ca^{2+} response evoked by TG2 alone (N=25 neurons; Wilcoxon signed-rank test: ****p<0.0001).

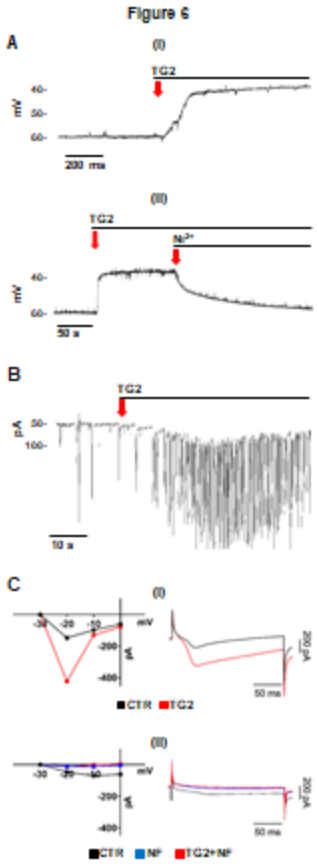

Figure 6. TG2 activates an inward calcium current through L-type VOCC membrane depolarization.

(A) Whole cell current clamp. (I) Addition of TG2 induced a slow membrane depolarization of about 20 mV (N=3). (II) Addition of Nickel after TG2 re-established resting membrane potential.

(B) Voltage clamp. TG2 perfusion promoted excitatory postsynaptic currents (EPSCs) consistent with the activation of an inward Ca^{2+} current (N=3).

(C) Whole cell voltage clamp results expressed as current/voltage (I/V) curves. (I) Perfusion of TG2 (red I/V curve) led to an increased inward current compared to control (black I/V curve). The graph on the right shows current recordings of the same experiment at -20 mV. The protocol for isolation of L-type VOCCs was applied as described in the Methods. (II) In the presence of NF (blue I/V curve), TG2 perfusion (red I/V curve, left panel) did not increase inward current compared to control (black I/V curve). The graph on the right shows current recordings of the same experiment at -20 mV (N=3).

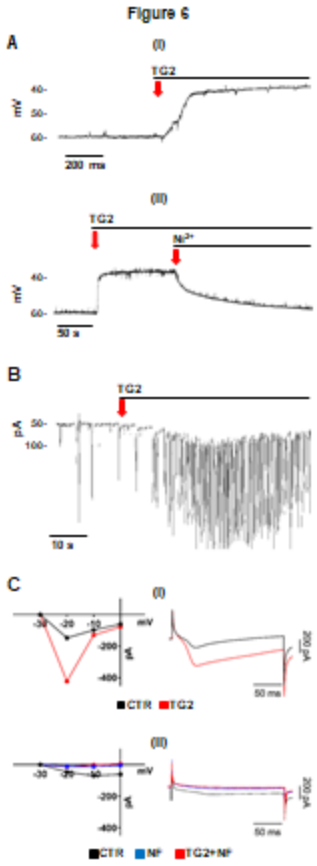

Figure 7. Contribution of NCX to TG2-dependent calcium rise.

(A) Temporal analysis of $[Ca^{2+}]_i$ changes in 14-20 DIV neurons exposed to exogenous TG2. Addition of TG2 in Na^+-free KRH led to an 8-fold increase in average Ca^{2+} influx compared to normal KRH (N=20 neurons; Wilcoxon signed-rank test: ****p<0.0001). Data are expressed as mean ± SD normalized to TG2 AUC values.

(B) Representative temporal analysis of neuronal $[Ca^{2+}]_i$ responses evoked by TG2 in the absence and in the presence of the NCX inhibitor YM-244769 (10 min) in Na^+-free KRH. YM-244769 induced a significant decrease in TG2-dependent Ca^{2+} influx. The graph shows mean TG2-induced AUC ± SD after YM-244769 normalized to TG2 alone in normal KRH (N=25 neurons; Wilcoxon signed-rank test: ****p<0.0001) and Na^+-free KRH (N=21 neurons; Wilcoxon signed-rank test: ****p<0.0001).

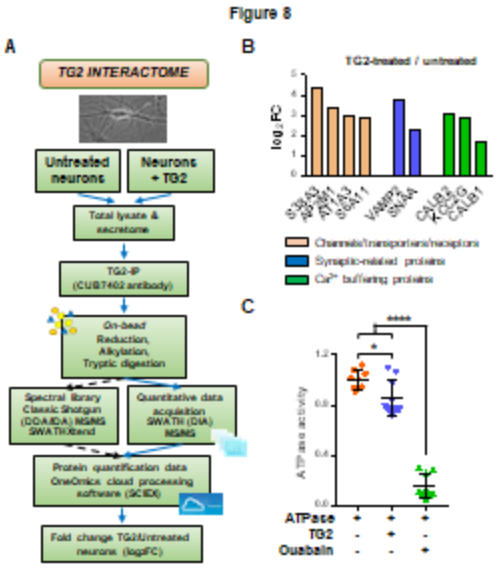

Figure 8. TG2 interactors in the neuronal extracellular environment: inhibition of Na^+/K^+-ATPase.

(A) Workflow of the identification of TG2-interactors. TG2 was immunoprecipitated from hippocampal neurons (total lysate including the secretome) incubated with extracellular TG2 or untreated (N=3 independent immunoprecipitations, from a neuronal preparation derived from ≥10 rat E18 embryos). TG2 co-precipitated proteins (TG2-IP) were trypsin digested on beads and analyzed by SWATH MS. SWATH quantitative data were extracted using a spectral library produced by shotgun/data dependent acquisition (DDA) MS on all TG2-IP samples.

(B) Selection of TG2 interactors shown according to logarithm of fold change (log_2FC) between neurons exposed to extracellular TG2 and untreated cells.

(C) The activity of porcine cerebral cortex ATPase (0.5 mU/well) assayed in the absence or presence of either gplTG2 (0.5 mU/well, 21.6 nM) or Ouabain (1 mM). Data are shown as mean ± SD of ATPase activity (mU/ml), normalized to ATPase alone values (N=3 independent experiments, one-way ANOVA test: *p<0.05; ****p<0.0001).

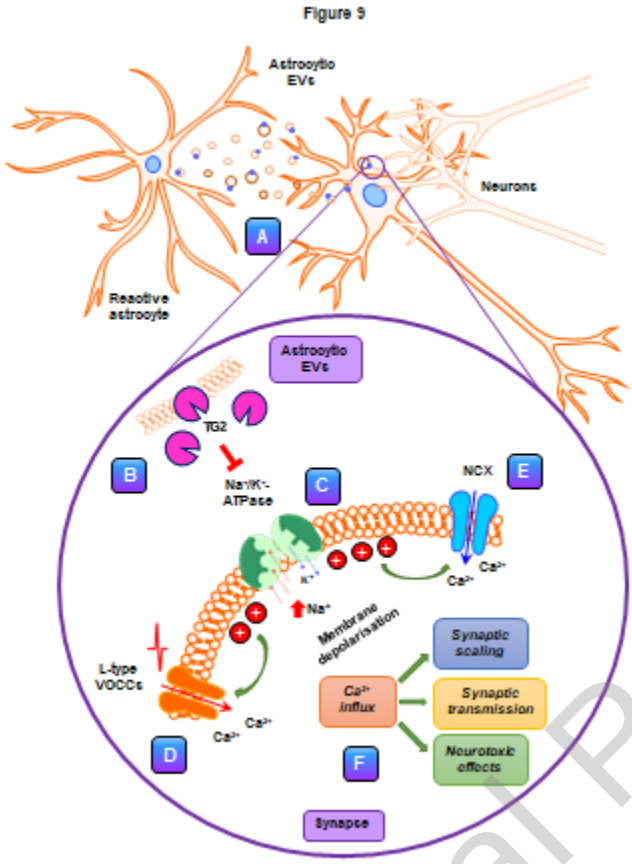

Figure 9. Schematic representation of the proposed mechanism.

(A) Activated astrocytes release EVs containing TG2 as a cargo and displayed at the EVs surface. (B) Extracellular TG2 (either astrocytes vesicle-bound or free in the medium) interacts with neurons and increases $[Ca^{2+}]_i$ via (C) inhibition of Na^+/K^+-ATPase, causing membrane depolarization (about 20 mV) and activation of an inward Ca^{2+} current through (D) L-type VOCCs and (E) the Na^+/Ca^{2+} exchanger (NCX) leading to (F) increase of $[Ca^{2+}]_i$ and Ca^{2+} dyshomeostasis.

Graphical abstract

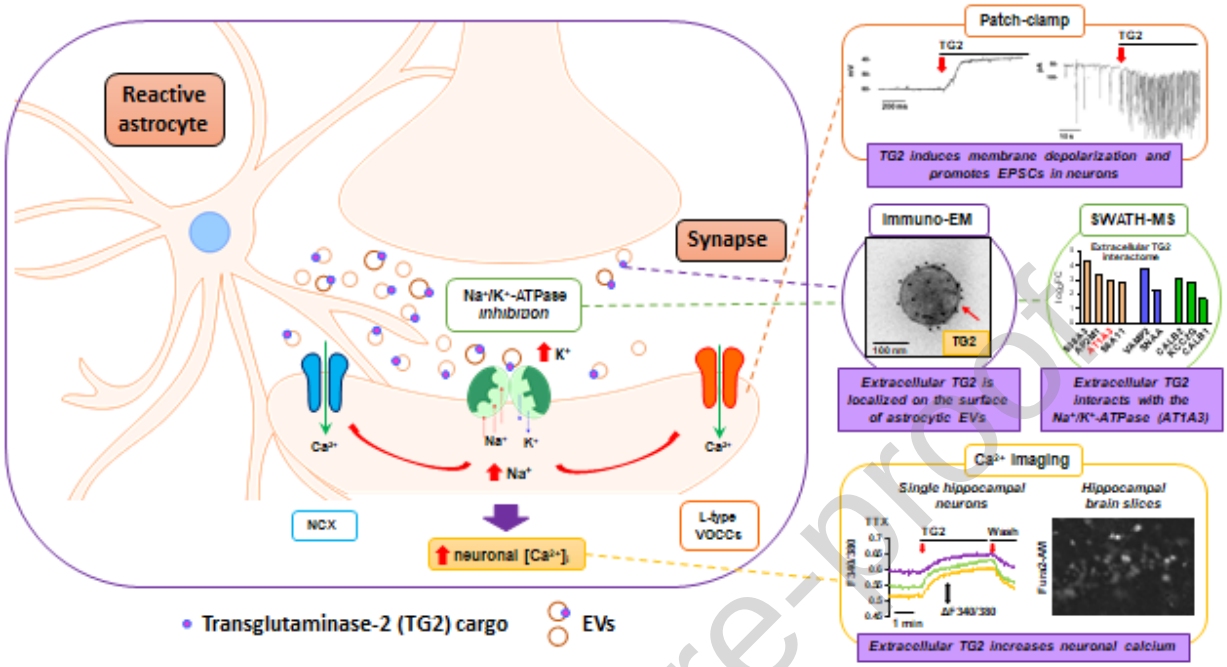

Highlights

- Primed astrocytes-derived EVs control neuronal $[Ca^{2+}]_i$ via TG2 as a surface-cargo
- Extracellular TG2 increases basal $[Ca^{2+}]_i$ in hippocampal neurons and brain slices
- TG2 mediates Na^+/K^+-ATPase inhibition, inducing VOCCs opening and NCX reverse mode
- Astrocytic EVs could affect synaptic activity in brain inflammation via TG2 cargo